

1 **NOvA Test Beam detector calibration**

2 **Technical Note**

3 **Robert Kralik**

University of Sussex

4 October 2, 2023

5 **Abstract**

6 The NOvA Test Beam detector calibration uses the same calibration procedure as the
7 standard NOvA detectors. The main aim is to remove differences in energy deposition
8 within the detector and to provide an absolute energy scale from collected charge to phys-
9 ical energy units. This allows for a direct comparison of the deposited energy in the Test
10 Beam detector with the standard NOvA detectors. On top of that, the unique qualities of
11 Test Beam allow us to use the Test Beam calibration to validate the calibration process and
12 possibly to provide a simulation-independent absolute energy scale.

13 Contents

| | | | |
|-----------|-------------------|---|-----------|
| 14 | 1 | Introduction | 3 |
| 15 | 2 | Overview of the Test Beam detector | 3 |
| 16 | 3 | NOvA calibration process | 6 |
| 17 | 3.1 | Relative calibration | 11 |
| 18 | 3.2 | Absolute calibration | 12 |
| 19 | 3.3 | Calibration uncertainties | 12 |
| 20 | 4 | NOvA Test Beam detector calibration | 12 |
| 21 | 4.1 | Fiber Brightness | 13 |
| 22 | 4.2 | Simulation | 14 |
| 23 | 4.3 | Threshold and shielding corrections | 15 |
| 24 | 4.4 | Period 1 | 15 |
| 25 | 4.5 | Period 2 | 18 |
| 26 | 4.6 | Period 3 | 24 |
| 27 | 4.7 | Period 4 | 30 |
| 28 | 4.8 | Absolute calibration results | 34 |
| 29 | 4.9 | Results | 34 |
| 30 | 4.10 | Validation | 34 |
| 31 | 5 | Conclusion | 49 |
| 32 | References | | 49 |

33 1 Introduction

34 TO DO: Write introduction. Why is TB calibration important and what it could achieve. Short
35 history of TB calibration. Mention Anna and Kevin.

36 2 Overview of the Test Beam detector

37 The NOvA Test Beam detector is a scaled down version of the near and far detectors shown on
38 figure 1. It is placed in the MC7b enclosure of the Fermilab Test Beam Facility in the path of
39 the MCenter beamline with a variety of beamline detectors to measure and identify a range of
40 particles with various momenta [1].

41 The Test Beam detector started with commissioning runs in May 2019 and ran, with an
42 exception of regular summer shutdowns, until July 2022, after which it was decommissioned.

The Test Beam data periods are:

| | | |
|----------|--------------------------------|-------------------------------|
| Period 1 | March 22 nd 2019 | - July 6 th 2019 |
| Period 2 | December 5 th 2019 | - March 20 th 2020 |
| Period 3 | January 12 th 2021 | - June 27 th 2021 |
| Period 4 | November 30 th 2021 | - July 10 th 2022 |

Table 1: Test Beam detector data taking periods.

43
44 Majority of the Test Beam detector and its instrumentation is identical to the other NOvA
45 detectors, with a few exceptions that could have an impact on the calibration. We are going to
46 identify and discuss these differences in this section.

47 General parameters

48 The NOvA Test Beam detector consists of two 31-plane blocks, each beginning and ending
49 with a vertical plane, with an additional horizontal plane glued inbetween them to preserve the
50 alternating pattern [2]. Each plane consists of 2 modules side-by-side, both made up of 32 cells.
51 Each cell is 2.6 m long with an inner (without the PVC) depth and width of 5.9 cm and 3.8 cm
52 respectively, same as for the other NOvA detectors. This brings the final dimensions of the Test
53 Beam detector to 63 planes \times 64 cells, or $2.6 \times 2.6 \times 4.1 \text{ m}^3$.

54 The 63 planes are numbered from 0 to 62, with even numbers corresponding to vertical
55 planes and odd numbers to horizontal planes. Cells are numbered 0 to 63, going from bottom
56 to top for horizontal planes and left to right, when facing the front of the detector, for vertical
57 planes.

58 The detector coordinate system is illustrated on figure 1. It is centered with (0,0,0) in the
59 centre of the first plane [3]. The x axis runs left to right when facing the front of the detector,
60 y axis bottom to top, and z axis goes along the beam direction from front to the back of the
61 detector. Position within each cell (w) is aligned with the x (y) axis for the horizontal (vertical)
62 cells, with $w = 0$ centered in the middle of each cell. The exact geometry of the Test Beam
63 detector was measured in several alignment surveys and is saved in gdml files [4].

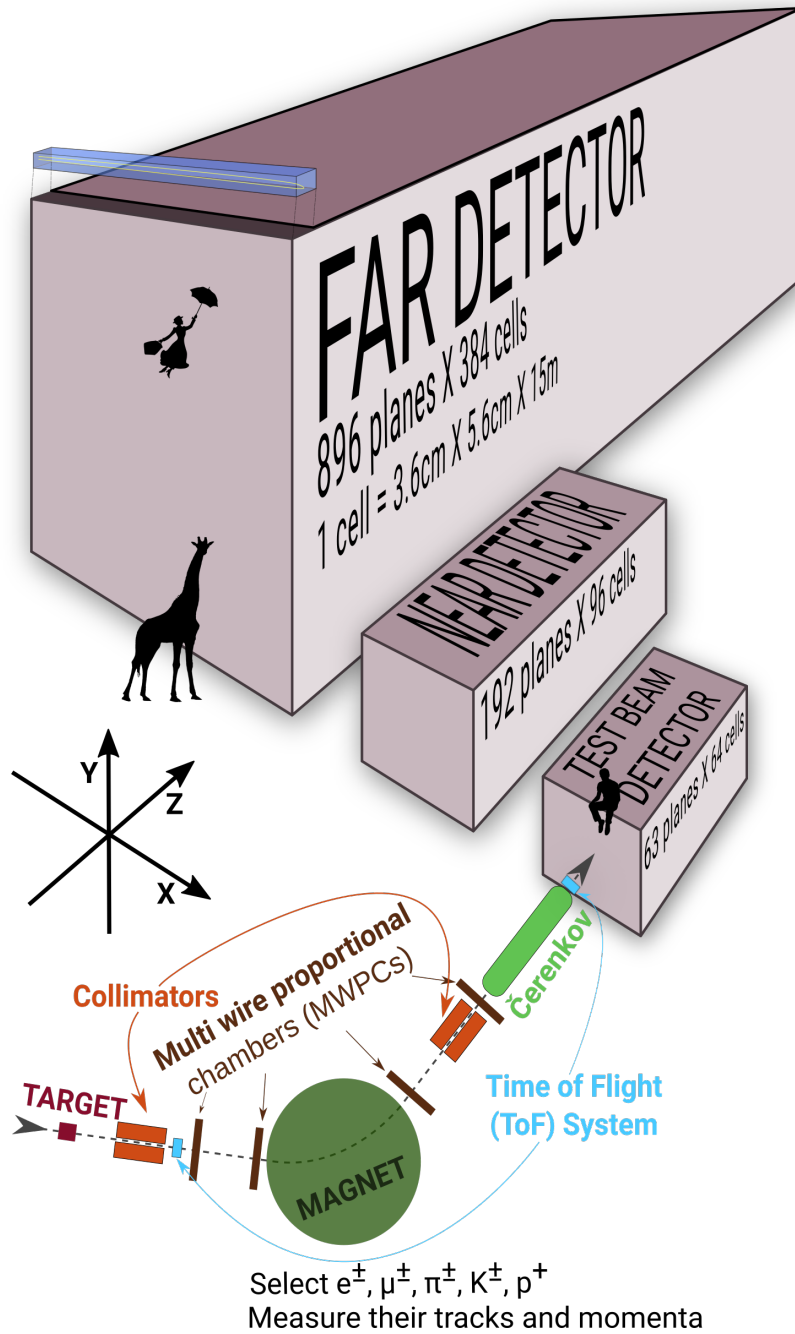


Figure 1: Comparison of Test Beam detector scale to the Near and Far NOvA detectors (and a man, giraffe, or Mary Poppins). Also shown are the Test Beam beamline detectors and components (not to scale), with arrows showing the direction of the beam. The three black arrows show the orientation fo the detector coordinate system.

In the past we encountered an issue when trying to align the Test Beam detector with the beamline measurements by rotating the detector. This broke several assumptions within the Test Beam geometry [3] and manifested as uncalibrated cells in the back of the detector [5]. This was fixed by realigning both the detector and the beamline separately, based on the last alignment survey, measured during the decommissioning of the detector. We implemented the

69 fix in the production tag R23-04-05-testbeam-production.a [3].

70 **Scintillator**

71 The Test Beam detector is filled with several different versions of the NOvA scintillator oil,
72 which differ mainly in the way they were stored since the filling of the near and far detectors.

73 This is illustrated on figure 2.

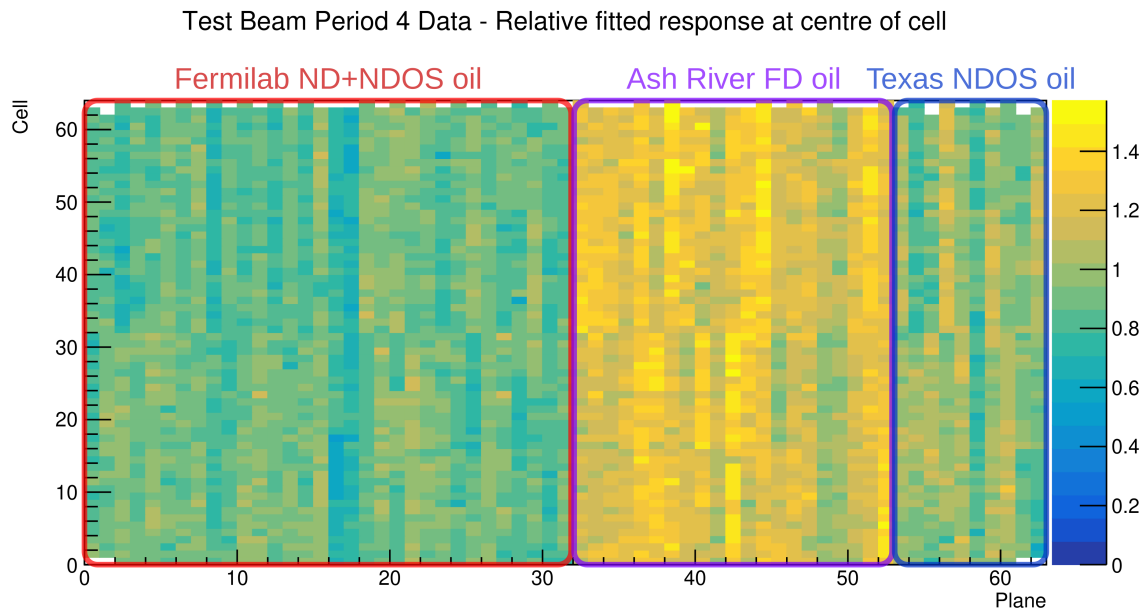


Figure 2: Uncorrected energy response in the centre of cells across the Test Beam detector showing a clear distinction between the different scintillator oils.

74 The original plan [6] was to use the scintillator from a tanker and one of the tanks located
75 outside at Fermilab. First tests showed acceptable results and the tanker oil was used to fill out
76 almost the entirety of the first block of the detector (first 32 planes) [7]. However, when we
77 loaded the oil from tank two into the tanker, it became extremely cloudy and unusable, possibly
78 due to contamination with water accumulated at the bottom of the tanks, which was mixed with
79 oil by the pump. The rest of the first block was topped up with high quality scintillator
80 from NDOS, which has been stored inside in barrels at MiniBooNE [8]. This is labeled as
81 "Fermilab ND+NDOS oil" on figure 2.

82 The first 21 planes of the second block (planes 32 to 52) were filled with the Far Detector
83 production scintillator shipped in from Ash River [9]. This oil has been stored in "totes" inside
84 a building and under several layers of black plastic [10]. We topped up these planes with the
85 NDOS scintillator [9].

86 The last 10 planes (planes 53 to 62) [9] were filled with scintillator drained from NDOS, but
87 stored in Texas A&M University and University of Texas at Austin [11, 12]. This scintillator
88 has higher light yield than the one from the tanker, but lower than the Ash River one [11].

89 In total the Test Beam detector is filled with 5418 gallons of scintillator oil with a weight
90 of approximately 28.6 tons [2].

91 **Readout**

92 The Test Beam detector uses in total 126 Front End Boards (FEBs), each reading out signal
93 from 32 cells (half of a plane) [2]. The readout is located on the top and right side (when
94 looking at the front) of the detector. 118 FEBs are version 4.1, same as in the Far Detector,
95 and 8 FEBs, located in pairs on planes 16, 17, 48 and 49, are version 5.2, same as in the Near
96 Detector. The Near Detector FEBs are designed to read out data in a fester rate and we used a
97 mix of FEB types to study the difference in their response and to validate both versions in the
98 same environment [13].

99 **Environment**

100 Unlike the near and the far detector, the Test Beam detector does not have any overburden to
101 shield it from cosmic particles, which affects their rate and energies inside the detector. There
102 is also less precise control of temperature and humidity than in the other detectors [source?],
103 which can potentially impact the scintillator and readout performance.

104 **Underfilled cells issue**

105 The Test Beam detector is slightly tilted around the Z axis by about 0.7° towards the readout.
106 This caused the top cells of both modules of all the horizontal planes (cells 31 and 63) to be
107 underfilled, creating an air bubble on the left side of the detector and severly affecting the energy
108 response in those cells [13]. This has been fixed [14] during the period 3 running by adding
109 extensions to the filling ports and overfilling the horizontal cells with the NDOS scintillator
110 stored.

111

3 NOvA calibration process

112 Test Beam is following the same ideas and procedures as the standard NOvA calibration. This
113 section intends to provide only a brief overview of the NOvA calibration. Further details can
114 be found in the other NOvA calibration technical notes [15].

115 The purpose of calibration is to make sure that we get the same amount of energy wherever
116 or whenever it's deposited in whichever of NOvA's detectors and to express this energy in phys-
117 ical units. The NOvA calibration uses cosmic ray muons, which provide a consistent, abundant
118 and well-understood source of energy deposition and consists of two closely connected parts
119 [16]:

- 120 1. The **relative calibration** corrects for attenuation of scintillator light as it travels through
121 the cell to the readout, as well as for differences between detector cells.
- 122 2. This is followed by the **absolute calibration**, which only uses stopping muons when they
123 are minimum ionising particles and calculates a scale between the measured charge read-
124 out, corrected by the relative calibration, and the simulated energy deposition in physical
125 units of MeV. This scale is calculated for each time period and each detector separately,
126 which ensures the energy deposition is directly comparable wherever or whenever it oc-
127 cured.

¹²⁸ There is also **timing calibration**, which corrects for the time differences of the signal to be
¹²⁹ processed and is done as a separate project to the relative and absolute calibrations and is out
¹³⁰ of scope of this technical note [17].

¹³¹ The units and variables used to define energy deposited in NOvA detectors are listed in table 2:

| | |
|--------|--|
| ADC | The digitized charge collected by the APDs from the Analog to Digital Converter [18]. |
| PE | Number of Photo Electrons. Calculated by a simple rescaling of the best estimate of the peak ADC. The PE per ADC scale only depends on the FEB type and the APD gain settings. This is technically done before the calibration and serves as the base unit for calibration. |
| PECorr | Corrected PE after applying the relative calibration results. The correction is a ratio between an average energy response (a pre-determined semi-arbitrary number) and the result of the the relative calibration fit (also called attenuation fit), which depends on w, cell, plane, epoch and detector. This makes the energy response equivalent across each detector. |
| MEU | Muon Energy Unit is the mean detector response to a stopping cosmic minimum ionising muon. Mean MeV/cm or mean PECorr/cm |
| MeV | Estimated energy deposited in the scintillator calculated from PECorr using the results of the absolute calibration. Additional correction for dead material needs to be made in order to get a calorimetric energy estimate. |

Table 2: Definitions of variables commonly used in calibration [15, 16].

¹³²

The final result of the NOvA calibration is the deposited energy in terms of physical units, which is in effect calculated as:

$$E_{dep}[\text{MeV}] = \underbrace{\frac{\text{MEU}_{truth}[\text{MeV}/\text{cm}]}{\text{MEU}_{reco}[\text{PECorr}/\text{cm}]}}_{\text{Absolute calibration} \atop (\text{Detector, epoch})} \times \underbrace{\frac{\text{Average response[PECorr]}}{\text{Fitted response[PE]}}}_{\text{Relative calibration} \atop (\text{Detector, epoch, plane, cell, w})} \times \underbrace{\left[\frac{\text{PE}}{\text{ADC}} \right]}_{\text{Scale} \atop (\text{APD Gain, FEB})} \times \text{Signal[ADC]}, \quad (1)$$

¹³³ where both the relative calibration results (blue fraction) and the absolute calibration results
¹³⁴ (red fraction) are stored in a database and applied together with the ADC-to-PE scale by the
¹³⁵ NOvASoft *Calibrator* package during processing of every hit in the NOvA detectors.

¹³⁶ Creating calibration samples

¹³⁷ To select good quality cosmic ray muons we first remove beam related events based on their
¹³⁸ time stamp relative to the time of the beam spill, as shown on figure 4. Then we apply basic
¹³⁹ reconstruction and track-based selection.

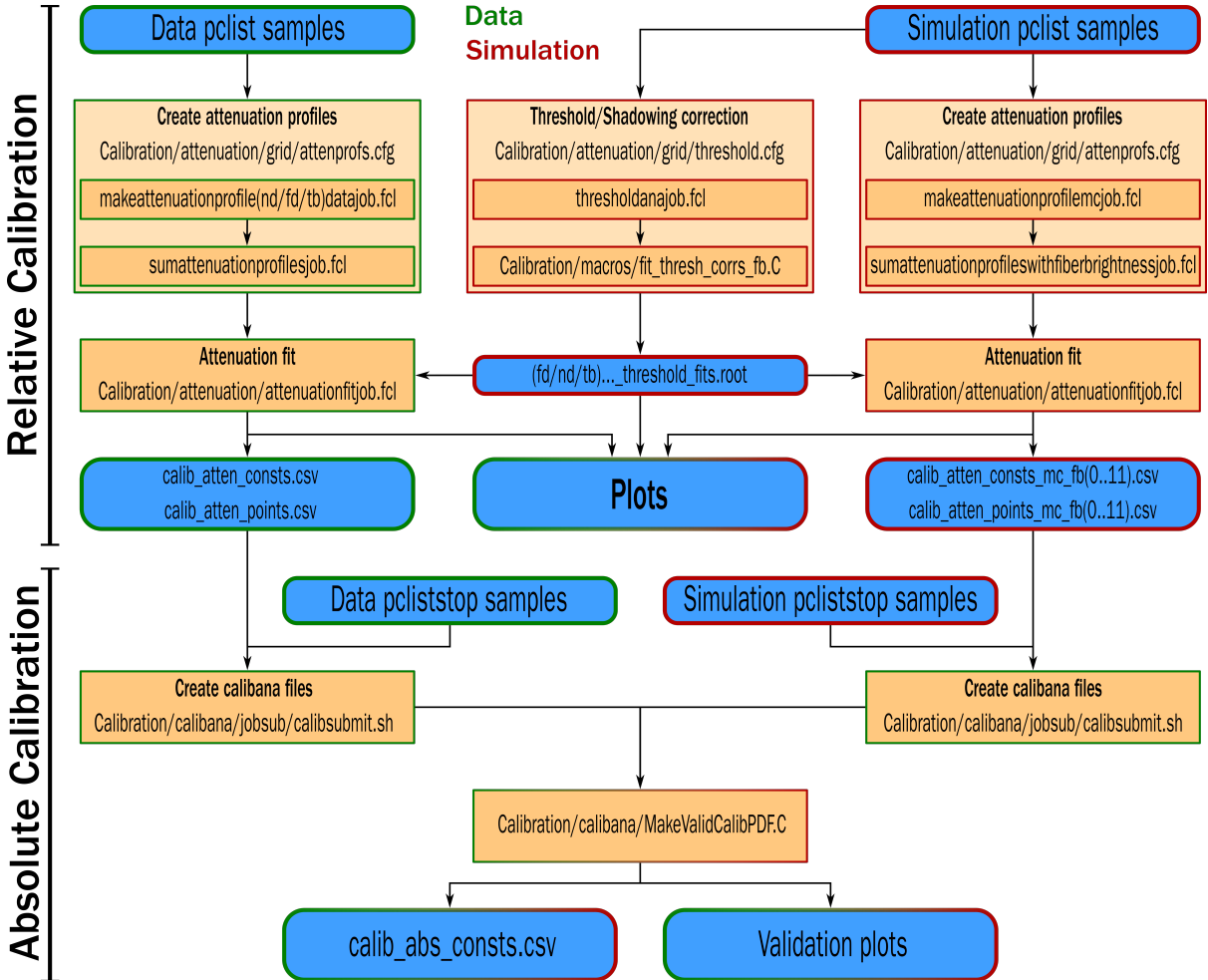


Figure 3: Flow chart showing the jobs (orange background) and files (blue background) needed and produced during the full NOvA calibration process. The left chain is showing the data calibration process (with green border) and is applied to every data calibration sample separately (periods or epochs). The center and right chains are showing the simulation calibration process (red border), which is redone only if there's a change to the detector simulation. The absolute calibration at the bottom combines data and simulation. The entire process is done separately for each NOvA detector.

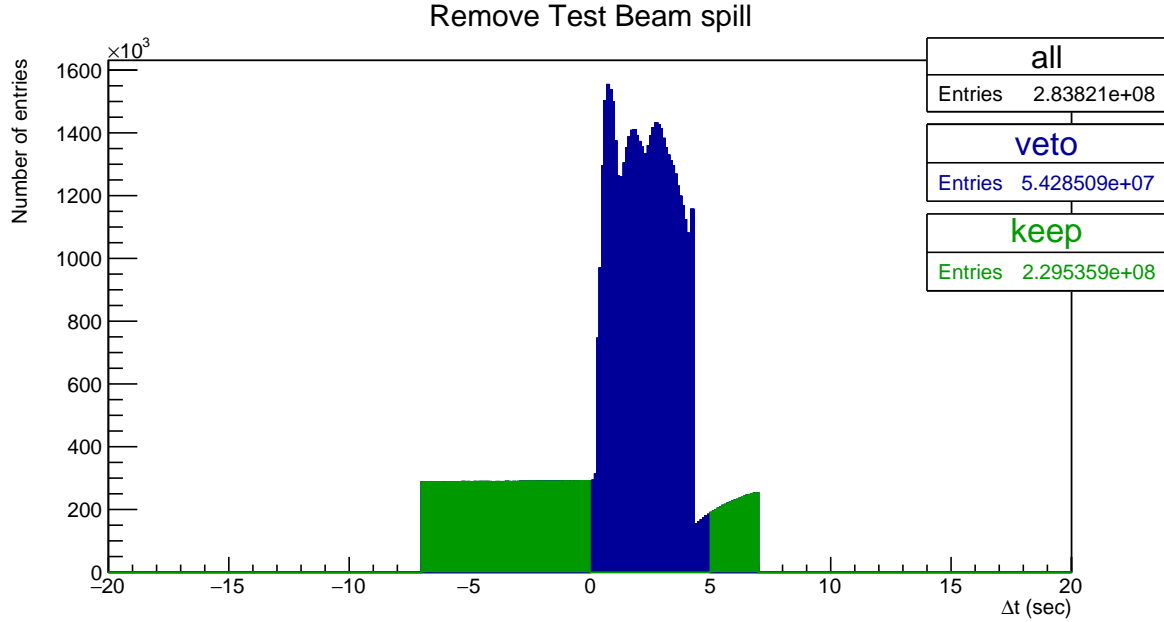


Figure 4: Test Beam beam spill events removed from the calibration samples. Test Beam beam spill is 4.2 seconds long and we remove events (in blue) within a 5 seconds window from the start of the beam spill. The remaining events (green) should mostly consist of cosmic particles. This example and the numbers of entries are for the full period 4 Test Beam sample.

140 Since energy deposition in a cell depends on the pathlength the particle traveled through
 141 the cell, we only use hits for which we can reliably calculate their pathlength. We call these
 142 hits **tricell** hits, as we require that all accepted hits also have a recorded hit in both neighboring
 143 cells of the same plane, as shown on figure 5. In case there's a bad channel in a neighboring
 144 cell, we ignore this channel and look one cell further. We can then calculate the pathlength
 145 simply as the cell width divided by the cosine of the direction angle [15, 16].

146 For the absolute calibration we select muons that stop in the detector. For this we identify
 147 muons with a Michel electron at the end of their track and only selection those [19].

148 For each data period/epoch and each simulation version we create two calibration samples
 149 that are used as the input for the relative and absolute calibration. The samples are called [20]

- 150 • pclist = **list** of pre-calibrated hist; Contains all selected cosmic muon events and is used
 151 in the relative calibration;
- 152 • pcliststop = pclist files only containing stopping muons used for the absolute calibration

153 **Fiber brightness**

154 For data, the relative calibration is done for each individual cell in each plane to properly
 155 account for any potential variations. Therefore we have to repeat the attenuation fit $N_{cell} \times$
 156 N_{plane} times. However, generating enough simulated events would be very computationally
 157 intensive. Additionally, we can assume that the simulated detector is approximately uniform
 158 plane to plane. Therefore, for simulation, we want to *consolidate* the detector planes and only
 159 consider variation in the two views and their cells, so repeat the fit $N_{cell} \times N_{view}$ times [21, 22].

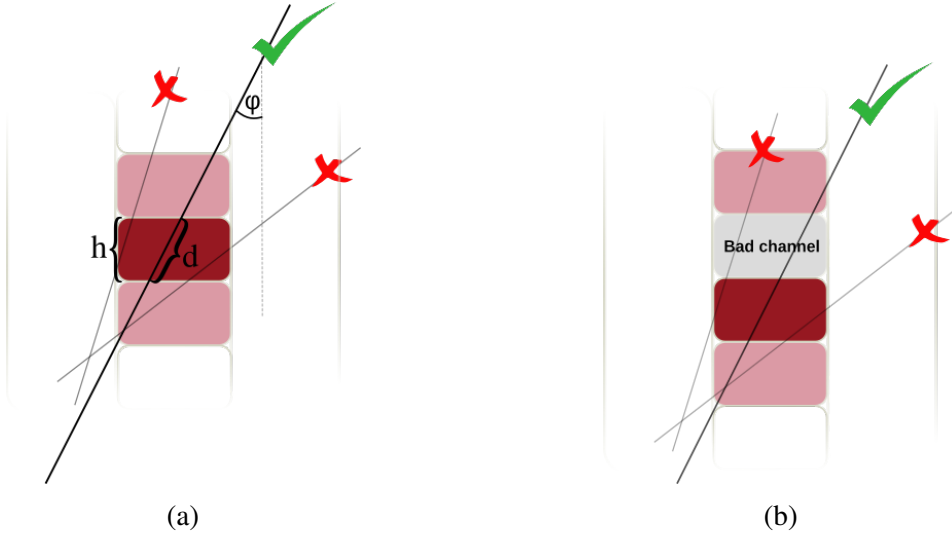


Figure 5: Illustration of the tricell condition (a). We only use hits that have two surrounding hits in the same plane to be used in the NOvA calibration. This is to ensure a good quality of the pathlength (d) reconstruction, which is calculated from the known cell height (h) and the reconstructed track angle (ϕ). In case the hit is next to a bad channel (b), we ignore this bad channel and require a hit in the next cell over.

160 There are some variations in the detector response cell by cell, that can be caused by different
 161 fiber brightnesses, but also by different qualities of the scintillator, air bubbles, APD gains,
 162 looped or zipped fibers and potentially others. To emulate these differences in the simulation
 163 without the need to simulate every cell individually and properly, we divide all the cells of
 164 each detector into 12 brightness bins, as shown on figure 6. These bins describe the relative
 165 differences in the detector response between individual cells [22]. Therefore in the end, for
 166 simulation we perform the attenuation fit in the $N_{view} \times N_{fiberbrightnessbin} \times N_{cell}$ phase space.

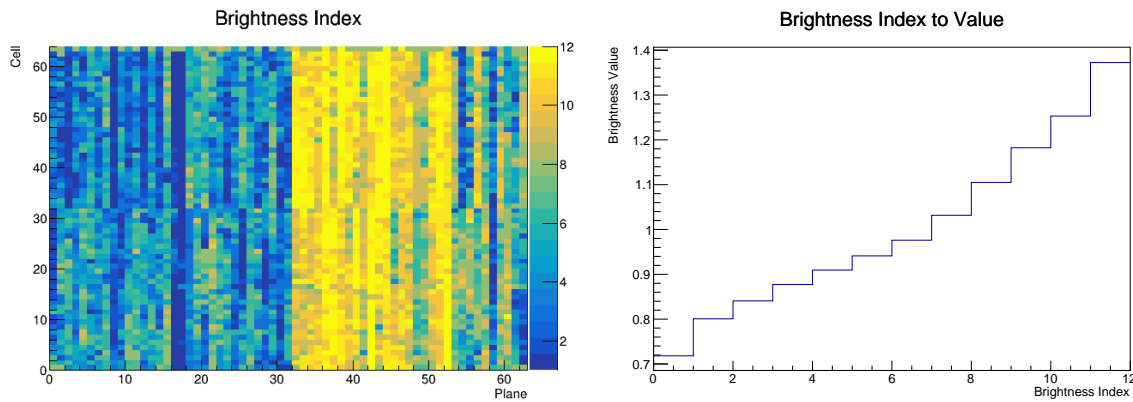


Figure 6: The Test Beam detector is (like the standard NOvA detectors) divided into 12 brightness bins (left plot), each representing a relative difference in energy response (right plot) due to different brightnesses of the fibers, scintillators, or readout.

167 TO DO: describe how do we create the brightness file

168 **Threshold and shielding correction**

169 Energy deposited far away from the readout may get attenuated enough to be shifted below
170 the threshold. These low energy depositions would be missing from the attenuation fit, biasing
171 it towards larger light levels going away from the readout. A similar effect, specifically for
172 the vertical cells, is caused by using cosmic muons for calibration. The top of the detector ef-
173 fectively shields the bottom of the detector, skewing the energy distribution of cosmic muons.
174 To correct for both of these effects, we use simulation to calculate the threshold and shield-
175 ing (also called threshold and shadowing) correction by comparing the true and reconstructed
176 information. We apply this correction before the attenuation fits [21].

177 **3.1 Relative calibration**

178 Relative calibration aims to create a fit, called *attenuation fit*, to the detector response over the
179 position in a cell separately for every cell inside each detector. Scaling the fitted response to
180 match the "average response" of the detector effectively removes relative differences through-
181 out and between all cells across the entire detector. This average response is a single number
182 chosen to approximately represent the average response in the middle of the cell. For the Far
183 Detector this number is 39.91 PE, for the Near Detector it's 37.51 and for Test Beam it's the
184 same as for the Far Detector 39.91. The scale of this number has no impact of this result as the
185 absolute scale of the detector response is determined during the absolute calibration [16, 21].

186 To create the attenuation fit we follow the following procedure [16]:

- 187 1. Create *attenuation profiles*, which are profile histograms of detector response in terms of
188 energy deposited per pathlength (PE/cm) as a function of position in the cell (w) through
189 each cell for all planes. We construct the attenuation profiles over a little wider range
190 than the actual length of the cell and always with 100 bins for each detector. This means
191 that smaller detectors, like the Test Beam detector, have a finer binning ($\sim 3\text{cm/bin}$)
192 compared to the Far Detector ($\sim 18\text{cm/bin}$).
- 193 2. Analyse the attenuation profiles. The job to create the attenuation profiles also creates
194 validation histograms, which should be analyzed prior to performing the attenuation fit
195 to make sure the attenuation profiles look as expected.
- 196 3. Apply the threshold and shielding correction that were created using the simulation plist
197 sample before the relative calibration.
- 198 4. Do the attenuation fit over the full length of each cell. The fit consists of
 - (a) exponential fit, which combines two cases. Light from the energy deposition travel-
ing straight to the readout, or going the opposite direction, looping around the cell
and then to the readout. The fitted function has a form:

$$y = C + A \left(\exp\left(\frac{w}{X}\right) + \exp\left(-\frac{L+w}{X}\right) \right), \quad (2)$$

199 where y is the response, L is the length of the cell and C , A and X are the fitted
200 parameters. X also represents the attenuation length.

201 (b) To remove the effect of residuals, mainly at the end of cells, we smooth out the
202 residuals from the exponential fit with LOcally WEighted Scatter plot Smoothing
203 (LOWESS).

204 5. Check the plots of the attenuation fit for a selection of cells.

205 6. Save the fit result to the database in the form of two csv tables. The *calib_atten_consts.csv*
206 table holds the results of the exponential fit, together with the final χ^2 of the fit. The
207 *calib_atten_points.csv* table holds the results of the LOWESS smoothing.

208 To ensure the quality of the attenuation fit, we only apply the results if the final $\chi^2 < 0.2$.
209 If $\chi^2 > 0.2$ we ignore the results for this cell and mark it as *uncalibrated*.

210 3.2 Absolute calibration

211 To find the absolute energy scale, we apply the relative calibration results on the stopping muon
212 sample and look at the energy they deposited in cells 1-2 meters from the end of their tracks.
213 In this track window they are minimum ionising particles and their energy deposition is almost
214 constant and well understood. We take a mean of their corrected deposited energy separate for
215 each view and for each calibrated sample. We then take the average over the two views to get
216 the final MEU_{reco}PECorr/cm for each sample [19].

217 From simulation we get the mean of the true energy deposited in scintillator MEU_{truth}MeV/cm
218 for the same sample of stopping muons. We ignore the energy that's lost in the dead material
219 (PVC extrusions) and deal with it separately. The absolute energy scale for each sample is then
220 the ratio of MEU_{truth}/MEU_{reco}. We save these absolute energy scales in another csv table called
221 *calib_abs_consts.csv* which stores the MEU values and their errors.

222 As part of the absolute calibration we also produce validation plots that show the effect of
223 calibration on the distribution of the stopping muons. We analyse these plots and if everything
224 looks all right load all the csv tables into the database.

225 3.3 Calibration uncertainties

226 WORK IN PROGRESS

227 4 NOvA Test Beam detector calibration

228 TO DO: list all the specific commands that need to be executed for the TB calibration. Like the
229 coloured table in the data based simulation.

230 The calibration samples used for the Test Beam detector calibration are listed in table 3.
231 We are using data from one of the Test Beam data-driven activity-based triggers. To produce
232 these samples we (or production) use the [prod_tb_ddactivity1_pclist_job.fcl](#) FHiCL file from
233 the novaprod/novaproduct/fcl/testbeam repository, or the corresponding mc file.

234 The calibration samples were originally created in keepups by the production, but due to a
235 fix to the Test Beam geometry, most of them had to be reproduced in 2023.

pclist samples

Data period 2:

```
prod_pclist_R23-04-05-testbeam-production.a_testbeam_ddactivity1_period2_v1
```

Data period 3:

```
prod_pclist_R23-04-05-testbeam-production.a_testbeam_ddactivity1_epoch3a_v1
```

```
prod_pclist_R23-04-05-testbeam-production.a_testbeam_ddactivity1_epoch3b_v1
```

```
prod_pclist_R23-04-05-testbeam-production.a_testbeam_ddactivity1_epoch3c_v1
```

```
pclist_testbeam_detector_activity_epoch3d_R21-01-28-testbeam-production.a
```

```
pclist_testbeam_detector_activity_epoch3e_R21-01-28-testbeam-production.a
```

Data period 4:

```
prod_pclist_R23-04-05-testbeam-production.a_testbeam_ddactivity1_period4_v1
```

Simulation:

```
rkrilik_pclist_testbeam_databasedsim_R23-04-05-testbeam-production.a
```

pcliststop samples

Data period 2:

```
prod_pcliststop_R23-04-05-testbeam-production.a_testbeam_ddactivity1_period2_v1
```

Data period 3:

```
prod_pcliststop_R23-04-05-testbeam-production.a_testbeam_ddactivity1_epoch3a_v1
```

```
prod_pcliststop_R23-04-05-testbeam-production.a_testbeam_ddactivity1_epoch3b_v1
```

```
prod_pcliststop_R23-04-05-testbeam-production.a_testbeam_ddactivity1_epoch3c_v1
```

```
pcliststop_testbeam_detector_activity_epoch3d_R21-01-28-testbeam-production.a
```

```
pcliststop_testbeam_detector_activity_epoch3e_R21-01-28-testbeam-production.a
```

Data period 4:

```
prod_pcliststop_R23-04-05-testbeam-production.a_testbeam_ddactivity1_period4_v1
```

Simulation:

```
rkrilik_pcliststop_testbeam_databasedsim_R23-04-05-testbeam-production.a
```

Table 3: SAMWEB definitions of the Test Beam calibration samples.

236 4.1 Fiber Brightness

237 To divide the Test Beam detector into fiber brightness bins we used the attenuation fit results
238 for period 4 data (described in section 4.7), since that is the best detector conditions data we
239 have. As we are only using the attenuation fit results in the centre of each cell, we've decided
240 to allow some cells that initially failed the calibration, to be still used for the creation of the
241 brightness file. As can be seen on figure 7, some attenuation fits have $\chi^2 > 0.2$, even though
242 they correctly represent the energy deposition in the centre of that cell. By carefully investigating
243 all cells with $\chi^2 > 0.2$ (possible for Test Beam, due to its small number of cells), we concluded
244 it is safe to use all attenuation fit results, for which $\chi^2 < 0.7$.

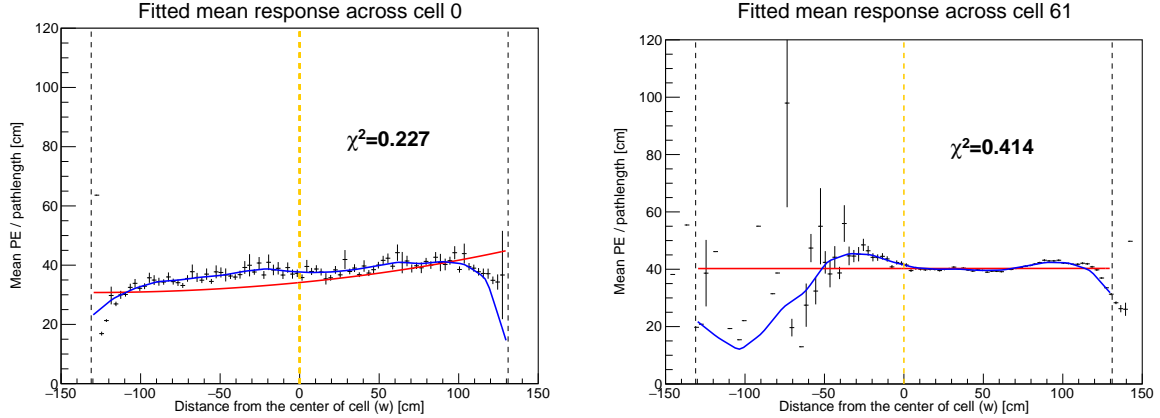


Figure 7: Attenuation fits for two cells that fail the calibration condition, but the fit (blue line) correctly represents the energy deposition in the centre of that cell (yellow dashed line).

4.2 Simulation

We used a data-based simulation of cosmic muons for the Test Beam detector calibration. The details are described in the Data-based simulation of cosmic muons (not only) for calibration technote [link to docdb]. We used half of period 4 data (used every second event as saved in the root file, therefore sampled from the entire period 4) as inputs and the newly created fiber brightness file to inform the simulation on the realistic detector conditions.

The distribution of events cosmic muon events from the new simulation is shown on figure

8.

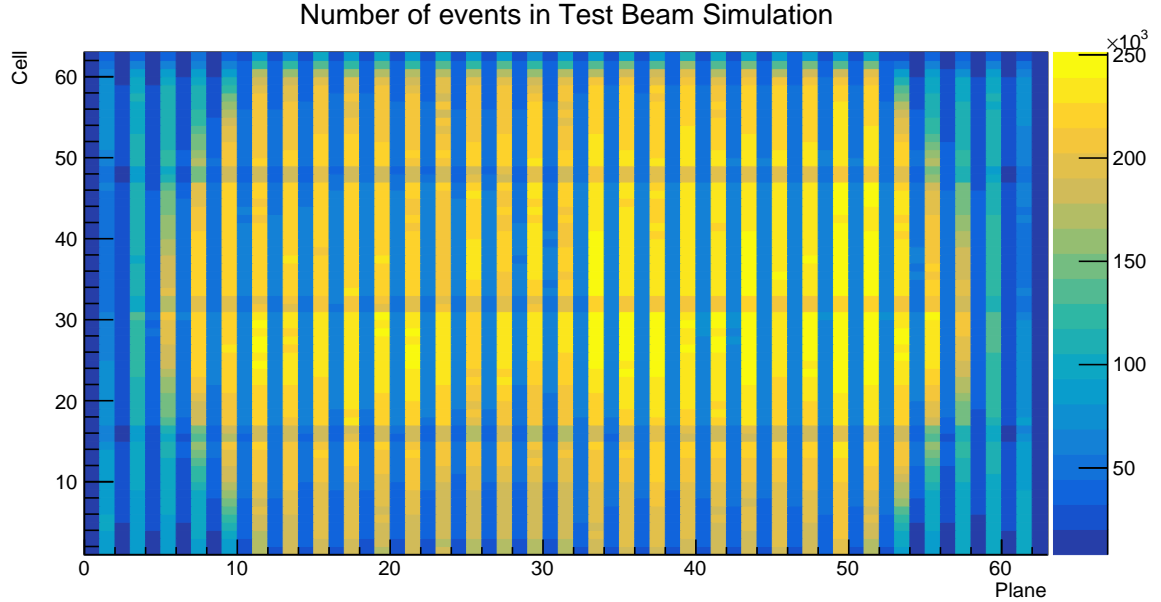


Figure 8: Distribution of events in the Test Beam simulation calibration sample.

The results of the attenuation fit are shown for each cell (in its centre) on figure 9. The blank cells show which cells failed the attenuation fit (their $\chi^2 > 0.2$). Most of the uncalibrated cells are on the edges of the detector, which is expected as those have much fewer events that

256 pass our selection than the rest. Examples of a standard detector response and of the response
257 for cells on the edge of the detector are shown of figure 10.

258 (I should explain here what is on the plots maybe - red is the exponential fit and blue is the
259 total with with the LOWESS. Most cells have the expected response of slow rise towards the
260 readout falling down on the edges).

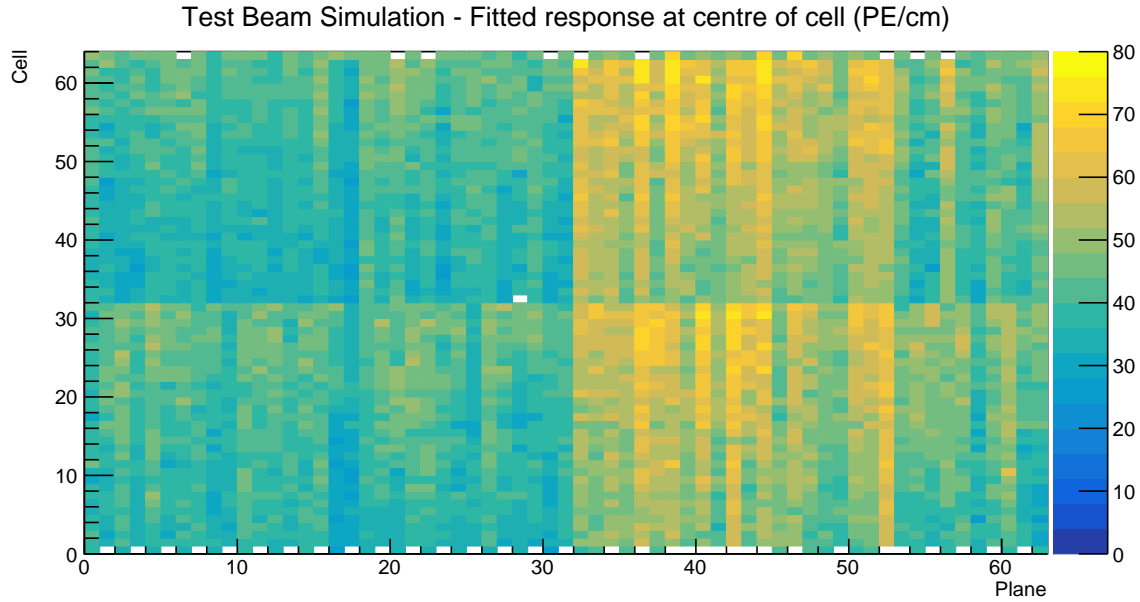


Figure 9: Overview of the attenuation fit results for the Teast Beam detector calibration simulation. Each cell represents the result fo the attenuation fit to the energy response in the centre of that cell. The blank cells are uncalibrated.

261 There is only one cell in the middle of the detector that is left uncalibrated, which is the cell
262 32 in a vertical plane in the brightness bin 5, shown on the top right of fig.10. The corresponding
263 $\chi^2 = 0.227$. It seems the reason the $\chi^2 > 0.2$ is an exceptionally high response with a large
264 uncertainty in the last bin.

265 This is a much better result of the relative calibration (attenuation fit) for a simulation than
266 the previous versions of Test Beam detector calibration simulations were able to accomplish.

267 **4.3 Threshold and shielding corrections**

268 The threshold and shielding correction for Test Beam is almost uniform across all cells as can
269 be seen on figure 11. This is expected as the hight of the Test Beam detector is 2.6 m has only
270 a negligible effect on the energy distribution of cosmic muons or on the threshold saturation.
271 The correction is basically just a normalization factor, except for the cell edges, but there is a
272 large variation in the energy response there anyway due to low number of events. Since the
273 relative calibration only cares about relative differences across the detector, a normalization
274 factor doesn't change anything.

275 **4.4 Period 1**

276 TO DO: add a description of period 1 data

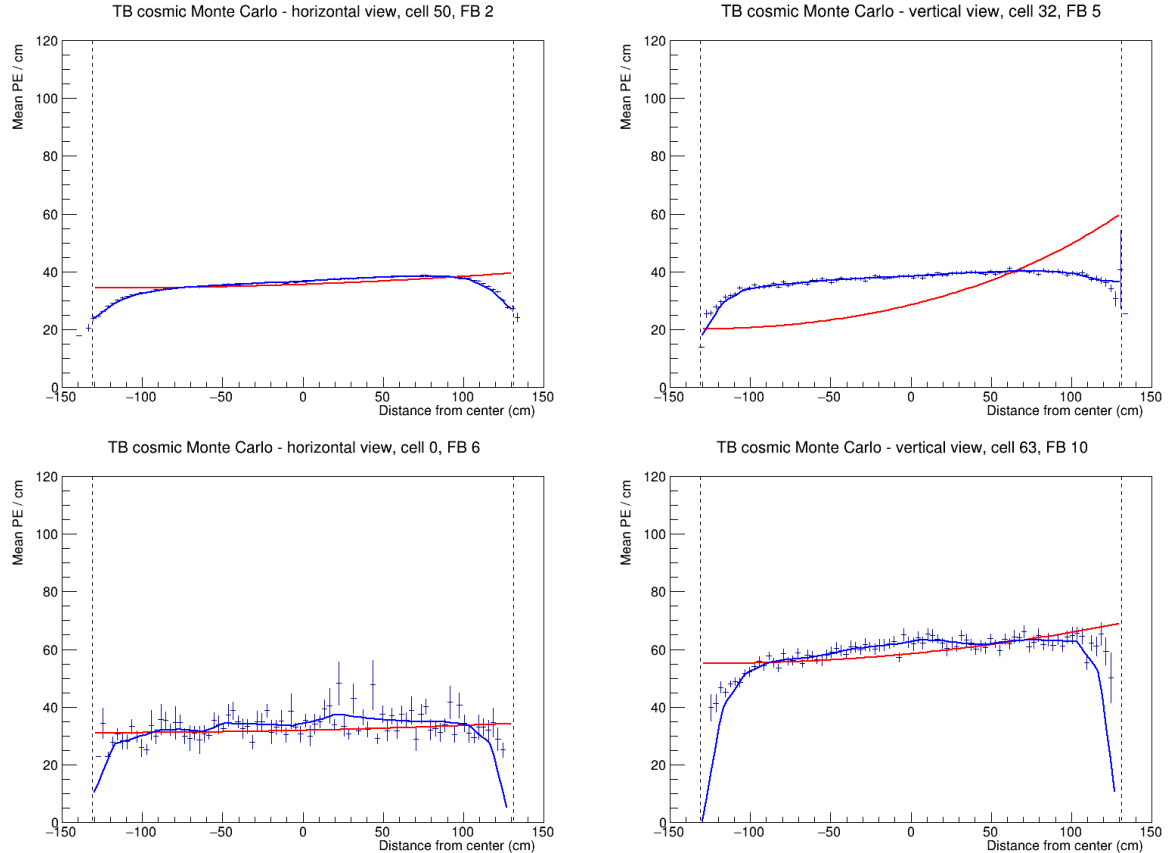


Figure 10: Attenuation fits for a selection of cells in the Test Beam calibration simulation. Top left is an example of a successful attenuation fit, top right is a failed fit due to statistical fluctuation in the last bin and the bottom plots show failed fits for cells on the edges of the detector.

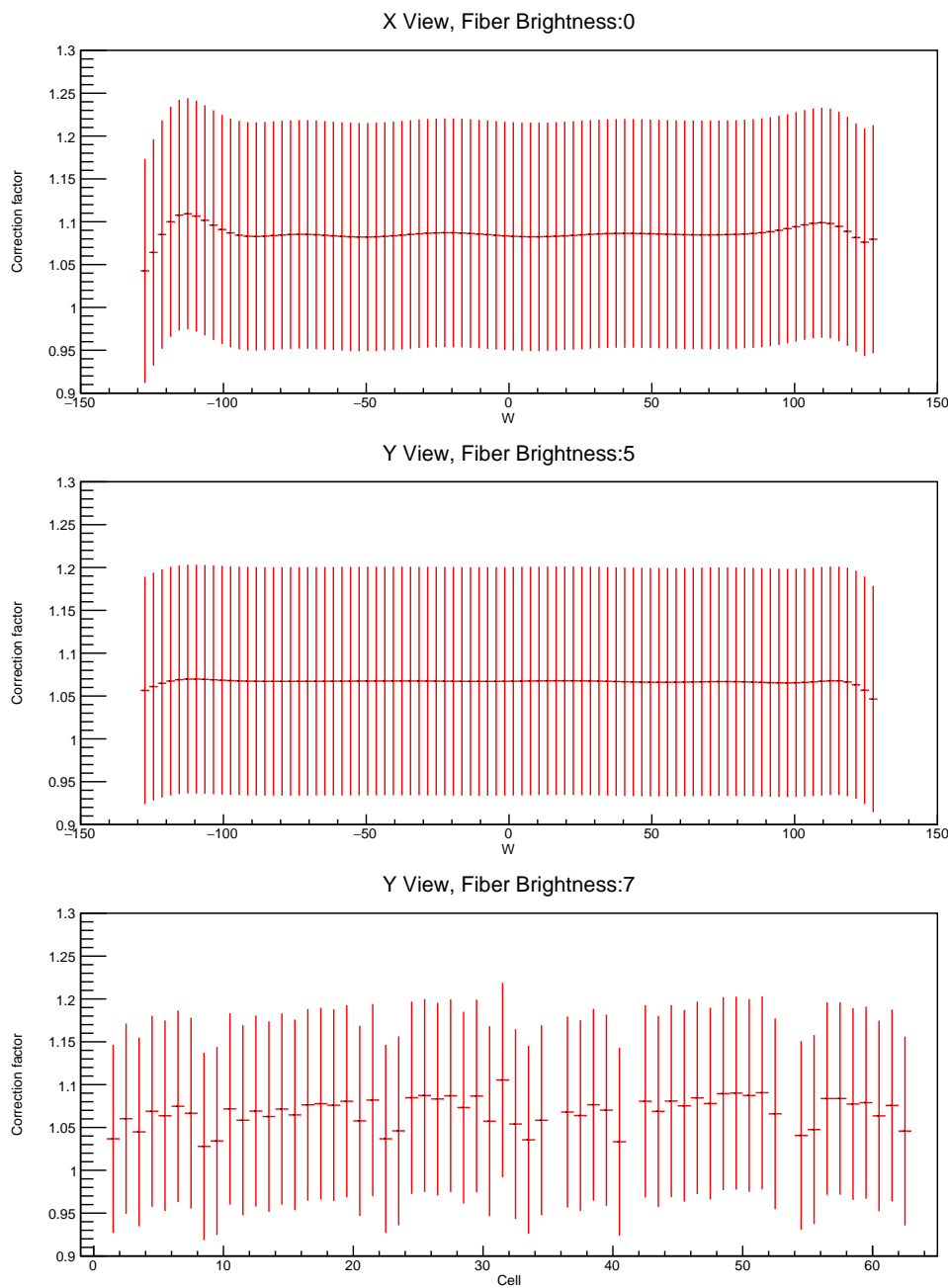


Figure 11: Examples of threshold and shielding corrections for the Test Beam detector

277 4.5 Period 2

278 The underfilled cells issue described in section 2 was present throughout period 2 data taking.
 279 This can be clearly seen on figure 12, represented by the empty cells 31 and 63 in the horizontal
 280 planes, which were marked as bad channels and therefore ignored during processing. This also
 281 affects the neighboring cells to the underfilled cells, which have fewer events due to the tricell
 282 condition.

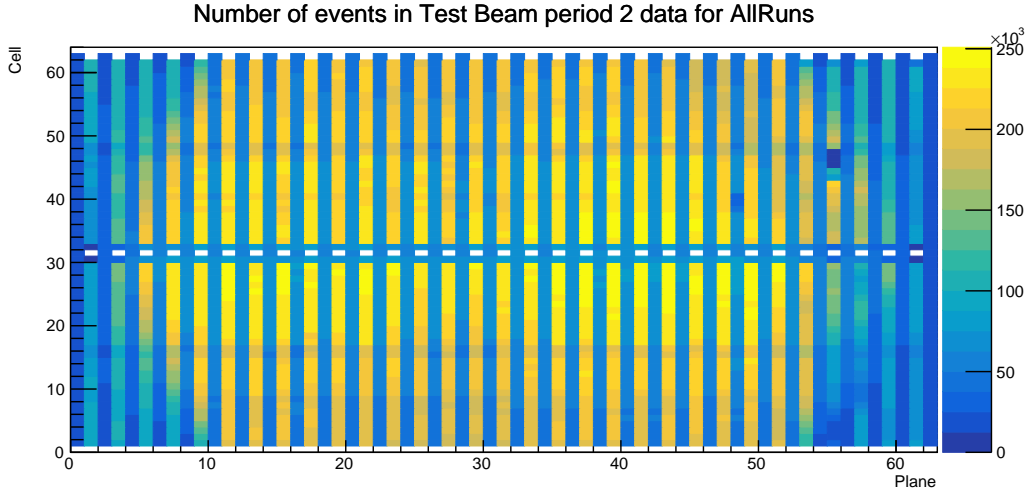


Figure 12: Distribution of events in the period 2 Test Beam data calibration sample.

283 There was also an issue of switched cables from the readout in plane 55 between cells 3
 284 and 46 [23], which can also be seen on figure 12. This is manifested as fewer total number of
 285 events in those cells and in their neighbours, again due to the tricell condition.

286 Officially, period 2 is divided into 6 epochs 2a - 2f, compared on figures 13, 14 and 15. The
 287 epochs mostly differ in the use of various FEB firmwares, with epoch 2c being a trigger study
 288 with paddles. As can be seen on the plots, the individual epochs vary only slightly, only in a
 289 small normalization. We decided to use the entire period 2 without splitting it into any smaller
 290 samples for calibration.

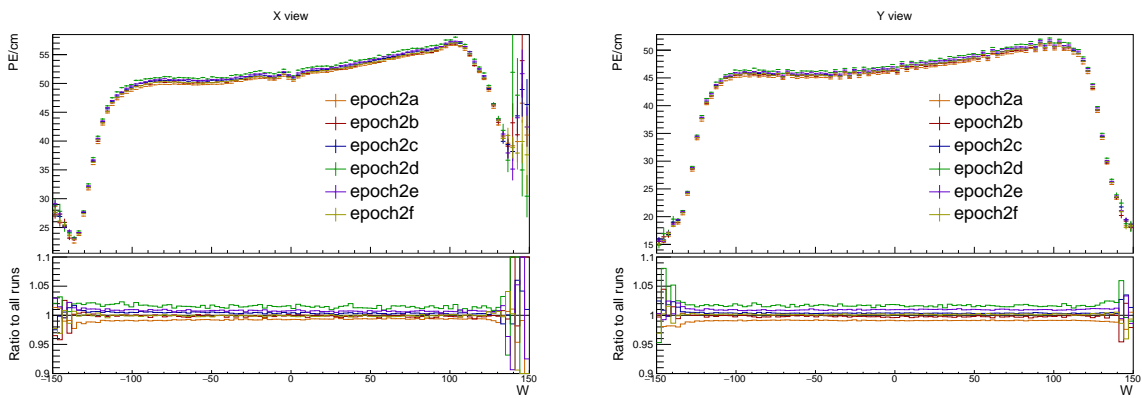


Figure 13: Uncorrected average energy response as a function of the position within a cell (w) for epochs in period 2. It is clear that there is no significant difference between the various epochs.

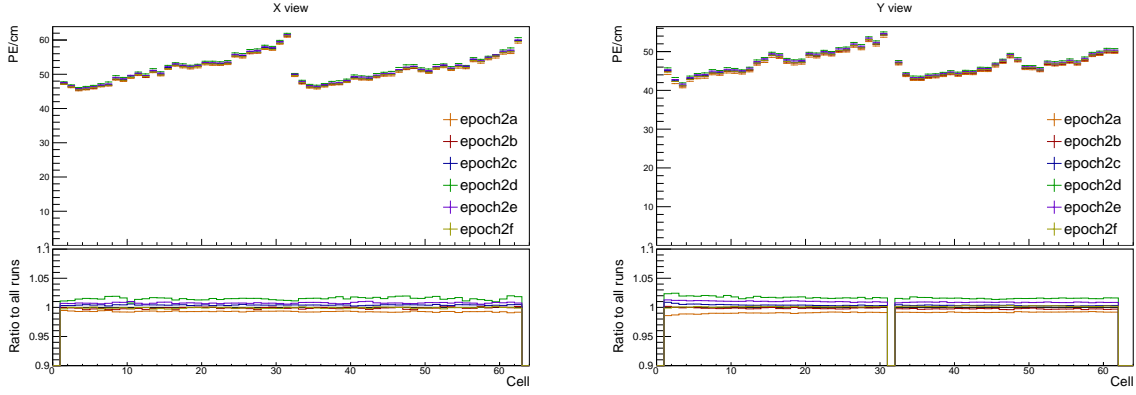


Figure 14: Uncorrected average energy response as a function of cells for epochs in period 2.

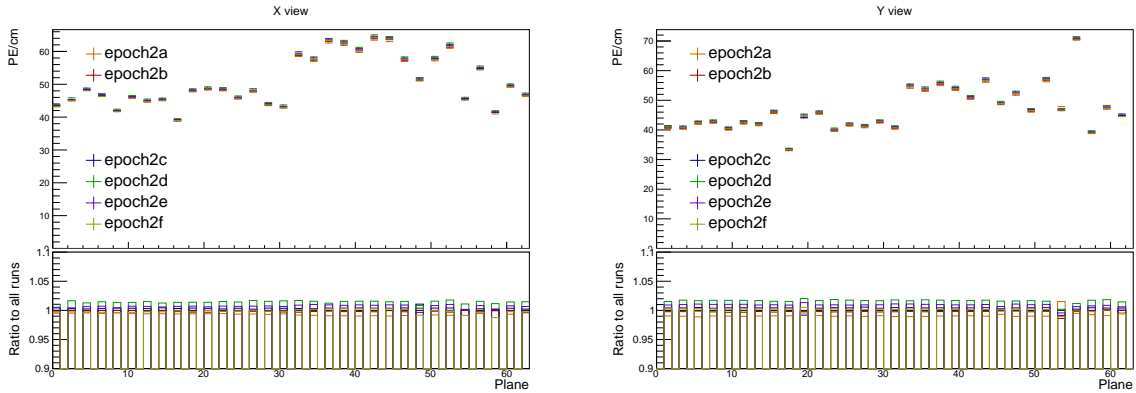


Figure 15: Uncorrected average energy response as a function of planes for epochs in period 2.

291 Period 2 relative calibration results

292 The results of the attenuation fit for period 2 are summarised on figure 16 showing the fitted
293 response at the centre of each cell, or blank cell if the cell failed calibration.

294 Most of the cells have the expected response, as shown on the left plot of figure 17. Here
295 the mean response in PE/cm slowly and approximately constantly rises towards the readout
296 (right side of the plot) and drops down on the cell edges, marked with dashed lines.

297 Some cells have a non-flat response across the cell, with one or more regions with lower en-
298 ergy response, as shown on the right plot of figure 17. These low regions are (almost certainly)
299 a real physical effect caused by zipped, or possibly even twisted fibers [24], present in all of
300 NOvA's detectors. Relative calibration corrects for this effect in data, but zipped fibers are not
301 included in simulation, for any of the detectors. This could potentially cause issues with the
302 ADC threshold in simulation.

303 Since the underfilled cells were marked as bad channels we didn't even attempt to calibrate
304 them. Their neighbours have fewer events due to the tricell condition but majority of them
305 pass the calibration condition, as shown on figure 18. The neighbouring cells in plane 1 don't
306 pass the calibration due to low statistics and therefore large fluctuations, as shown on figure 19.
307 This is likely due to a combination of the tricell condition and plane 1 being on the edge of the
308 detector, which typically has fewer (accepted) hits than the center as shown on figure 12.

309 The left half of plane 55 has $> 3 \times$ larger response than it's surrounding planes, as shown

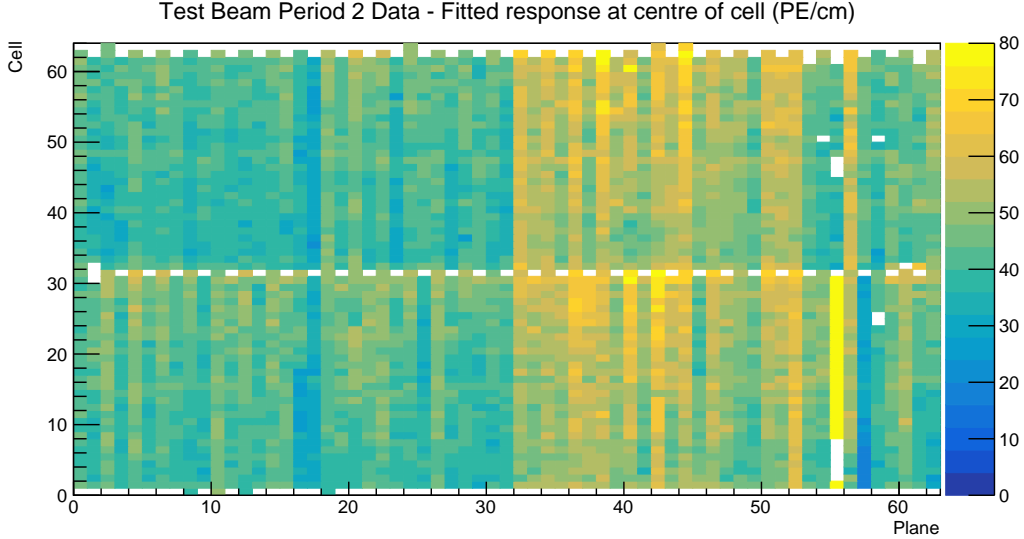


Figure 16: Overview of the relative calibration results for the Teast Beam detector period 2 data. Each cell represents the result of the attenuation fit to the energy response in the centre of that cell. The blank cells are uncalibrated.

310 on the left plot of figure 20. Similarly, the left half of plane 57 has lightly lower response than
 311 the surrounding planes, as shown on the right plot of figure 20. This is due to the corresponding
 312 APDs/FEBs faultly recording different energy response than the real energy deposited in the
 313 detector. Since this is present for all data, not only for the comsic muons used for calibration, it
 314 is important to correctly calibrate them. The issue can arrise if these FEBs have been "faulty"
 315 only for a limited time of the entire calibrated period. Since we are doing the attenuation fit on
 316 the profile histograms, if an FEB records a standard response for half of the time and $7\times$ larger
 317 response for the seconds half, calibration is going to assume the response was $4\times$ larger the
 318 entire time, which is incorrect. Since both of these planes are in the back of the detector, we
 319 decided to ignore this effect for period 2.

320 The swapped cables in plane 55 have almost no events, which affects both them and their
 321 neighbours as shown of figure 21.

322 Several cells in the end of the Test Beam detector are uncalibrated due to bins on the edges
 323 of the cell having an unusually high response, or no events at all, as shown on figure 22. It is
 324 unknown if this is a real physical effect, possibly related to the fibers, or unfiltered noise hits,
 325 or something else entirely. Since these cells are in the end of the detector, it is safe to ignore
 326 them.

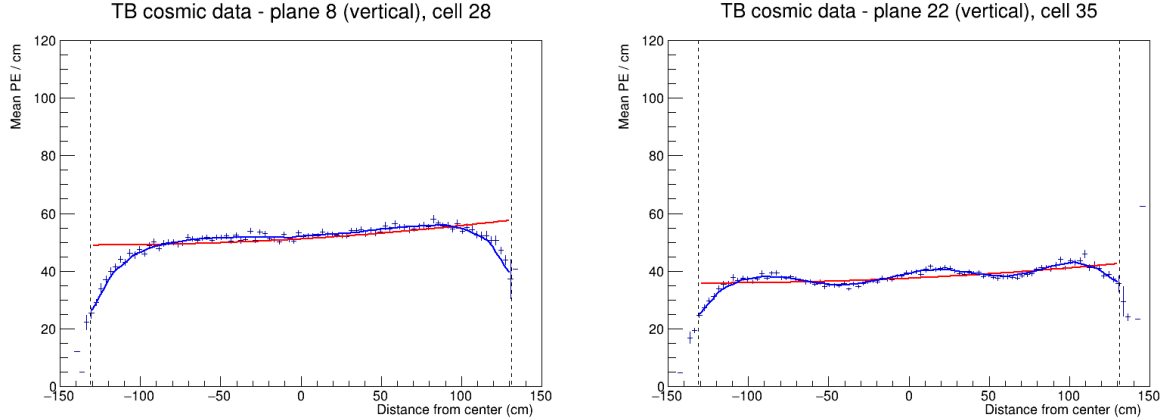


Figure 17: Attenuation fits for a selection of cells in period 2. Left plot shows an example of the standard energy deposition in the Test Beam. Right plot shows the effect of zipped fibers.

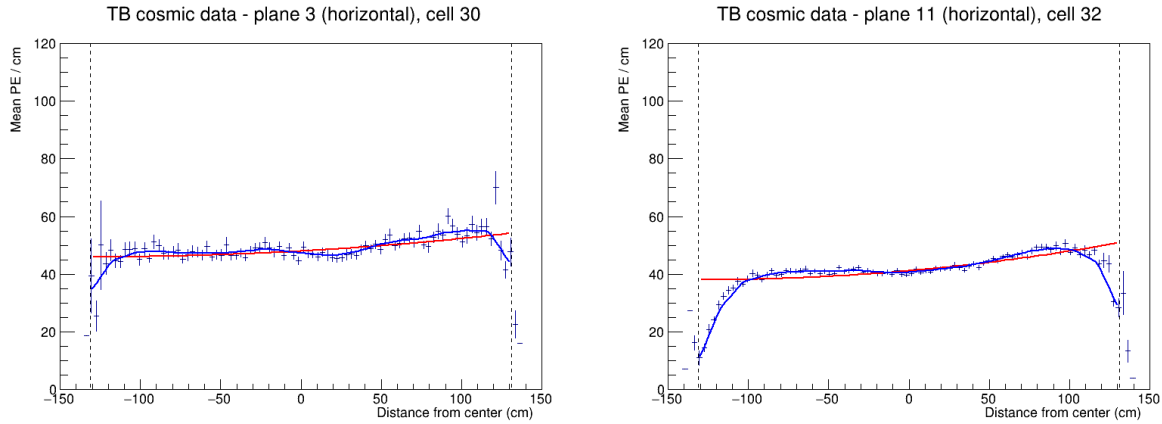


Figure 18: Fit to the energy response in period 2. The cells neighbouring the underfilled cells have fewer events and therefore larger fluctuations than the "usual" Test Beam cell.

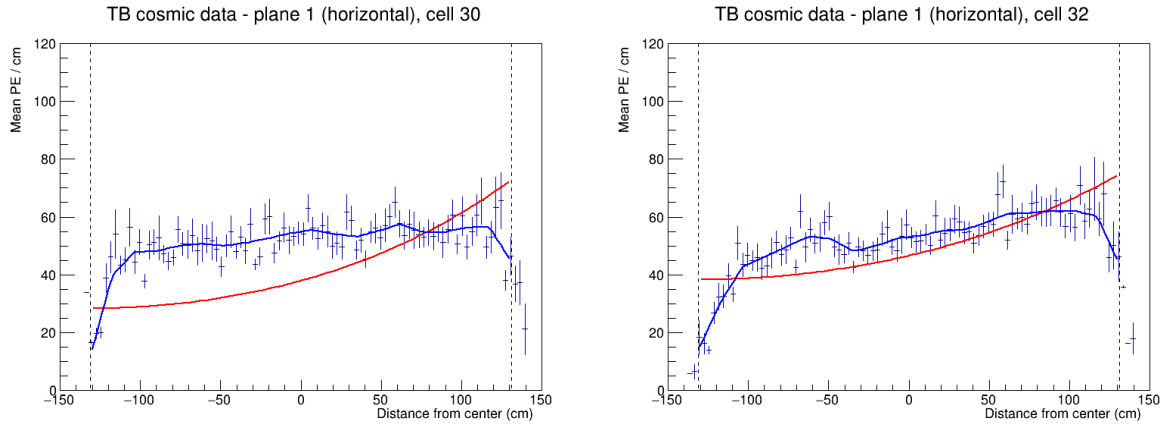


Figure 19: Fit to the energy response in period 2. The neighbouring cells to the underfilled cells in plane 1 are uncalibrated due to low statistics.

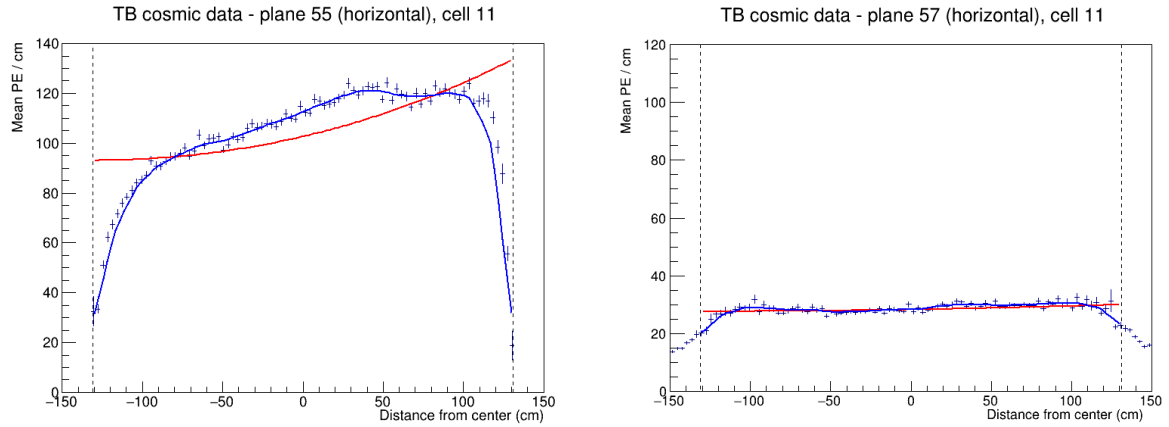


Figure 20: Fit to the energy response in period 2. Lower halfs of planes 55 and 57 have a different scale of energy response than the surrounding planes.

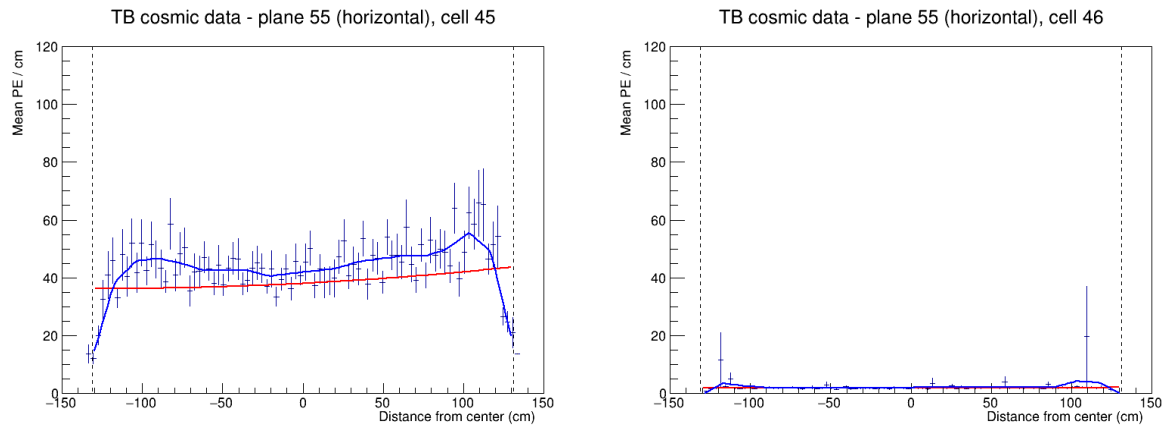


Figure 21: Fit to the energy response in period 2. Cells with swapped readout cables have almost no recorded events as shown on the right plot. This also affect their neighbouring cells due to the tricell condition as shown on the left plot.

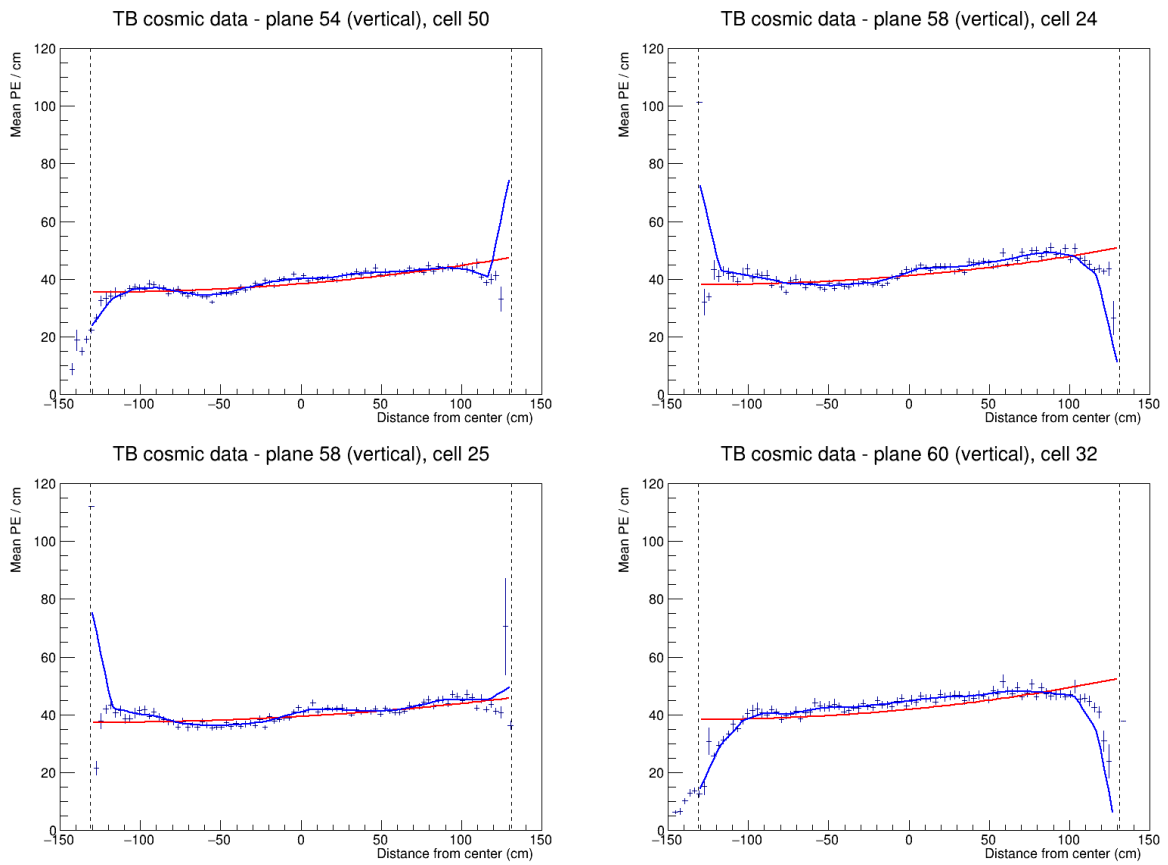


Figure 22: Fit to the energy response in period 2. Examples of cells that have an unusually high or low energy response at the edge of the cell. These cells are not calibrated.

327 4.6 Period 3

328 The underfilled cells were refilled (or overfilled) during the period 3 data taking. This was the
329 main motivation for dividing period 3 into individual epochs as shown on table 4. One more
330 major event that could impact the Test Beam data is the replacement of several faulty FEBs,
331 which motivated the creation of epoch 3e.

| | | |
|----------|-------------------------------|--|
| Epoch 3a | January 12 th 2021 | Underfilled cells |
| Epoch 3b | April 21 st 2021 | Overfilling the back 9 horizontal planes and the 7th horizontal plane from the front |
| Epoch 3c | April 27 th 2021 | Overfilling of the 15 front horizontal planes (except the 7th, which was already done) and the 14th horizontal plane |
| Epoch 3d | April 30 th 2021 | Overfilling of the remaining 8 horizontal planes |
| Epoch 3e | May 12 th 2021 | FEB swaps |

Table 4: Test Beam period 3 epochs, their start dates and the reason for their separation.

332 The refilling of the underfilled cells can be clearly seen on the cell hits distribution on figure
333 23 and on the distribution of energy deposition across horizontal cells (Y view) on figure 25.

334 From the cell hits distributions we can also see there are a few channels (cells) that were
335 likely dead for a certain time and weren't recording the same number of events as the surrounding
336 cells. This is specifically plane 48, cell 39 in all of period 3 and plane 18, cell 31 in epochs
337 3d and 3e.

338 The energy distributions across vertical cells and planes (X view) on figures 25 and 26
339 shows, that the top half of plane 58 has a very distinctly different energy deposition compared
340 to the rest of the cells, while having the same number of events, as can be seen on figure 23.
341 This is the most impactful of the faulty FEBs replaced for Epoch 3e.

342 From these discussions, we have decided to calibrate epochs 3a, 3b and 3c together (all
343 epochs containing any underfilled cells) and separately calibrated epochs 3d and 3e. The faulty
344 FEB in plane 58 is far enough in the back of the detector that we didn't find it necessary to
345 calibrate epochs 3d and 3e separately. Also epochs 3b and 3c only contain a few days worth of
346 data, which wouldn't be enough for a successful attenuation fit.

347 Combined epochs 3a, 3b and 3c relative calibration results

348 The results of the attenuation fit are summarised on figure 27 showing cell \times plane distribution
349 of the fitted response at the centre of each cell.

350 We can see that some of the underfilled cells that have been refilled for epochs 3b or 3c are
351 now calibrated thanks to including them into the same attenuation fit. An example of energy
352 deposition in such a cell is on the left plot of figure 28.

353 Same as in period 2 most of the neighbouring cells to the underfilled cells are calibrated,
354 except for cell 32 in plane 1, shown on the right of figure 28, which is also affected by the low
355 statistics at the edges of the detector.

356 There is a couple of notably faulty FEBs with a different energy response than their neighbours.
357 Besides the expected top half of plane 58, which has about 5 \times larger response than the

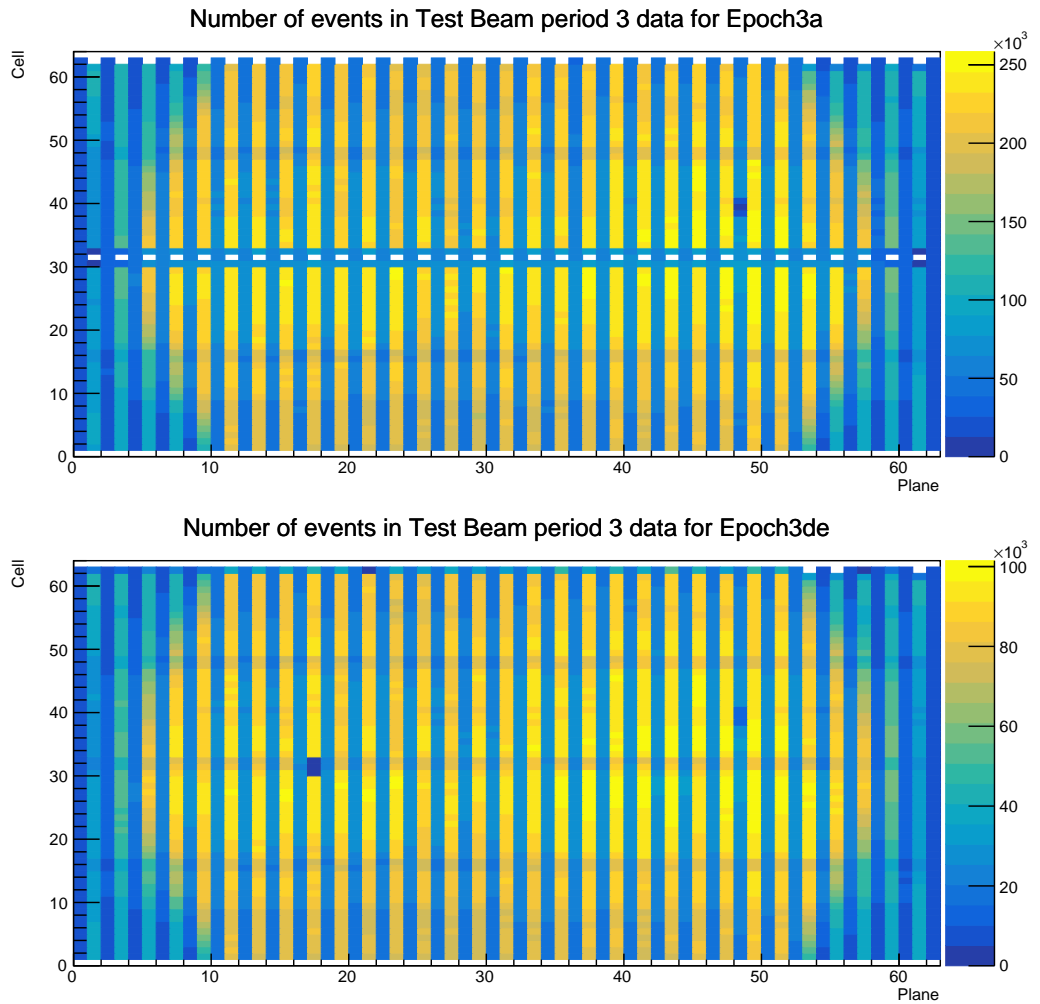


Figure 23: Distribution of events in the period 3 Test Beam data calibration sample. Comparison of Epoch 3a data before the refilling of the underfilled cells and Epoch 3de (combination of Epochs 3d and 3e) after the full refilling.

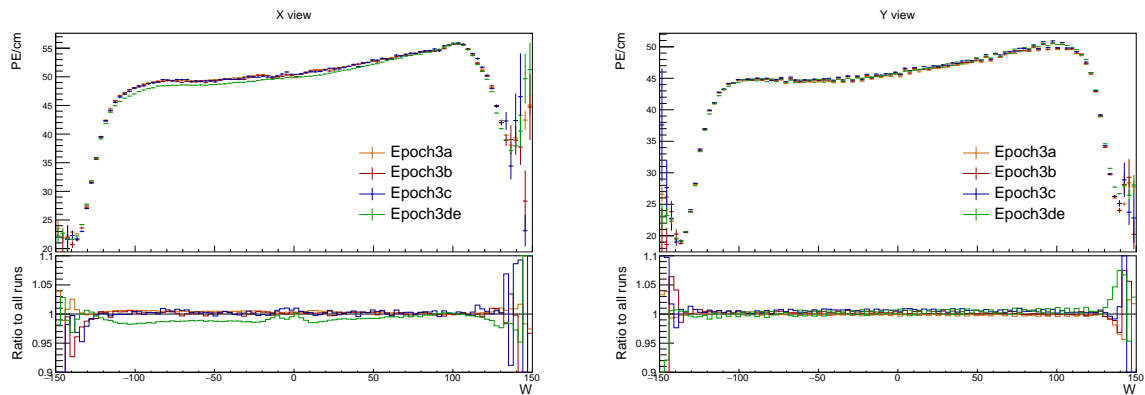


Figure 24: Uncorrected average energy response as a function of the position within a cell (w) for epochs in period 3.

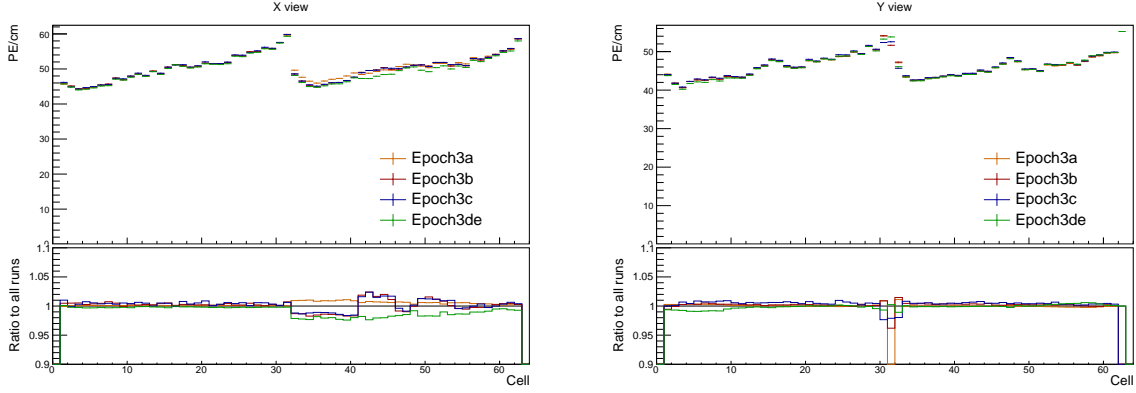


Figure 25: Uncorrected average energy response as a function of cells for epochs in period 3.

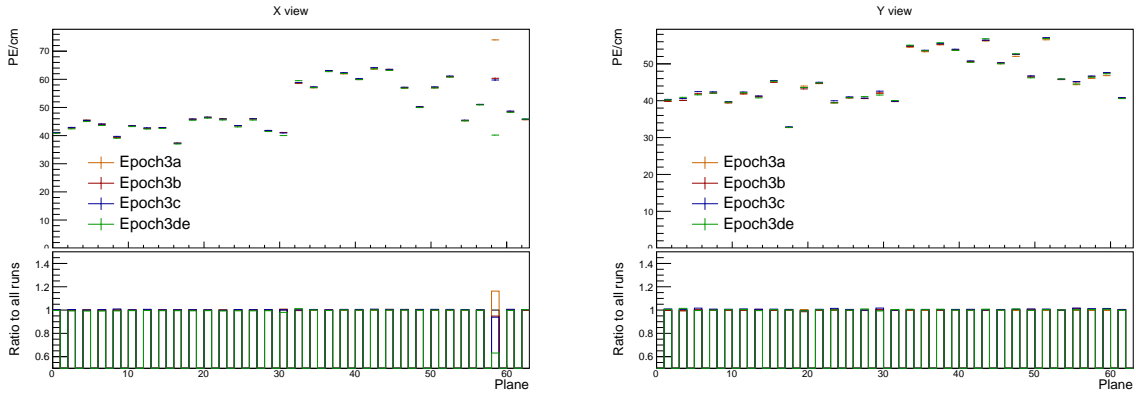


Figure 26: Uncorrected average energy response as a function of planes for epochs in period 3.

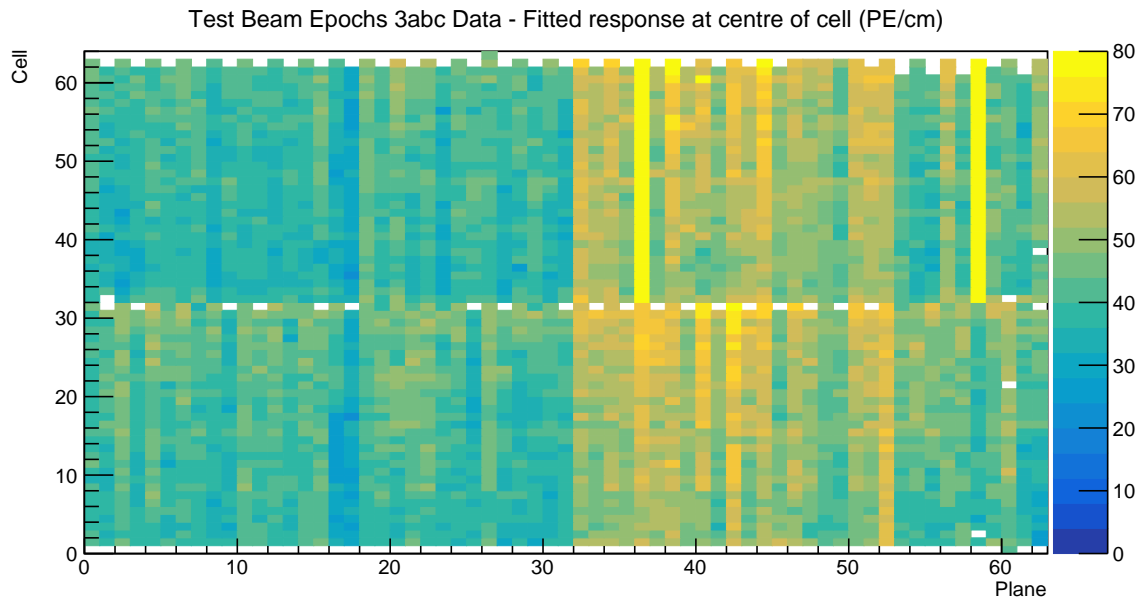


Figure 27: Overview of the relative calibration results for the Teast Beam detector period 3, combined epochs 3a, 3b and 3c data. Each cell represents the result fo the attenuation fit to the energy response in the centre of that cell. The blank cells are uncalibrated.

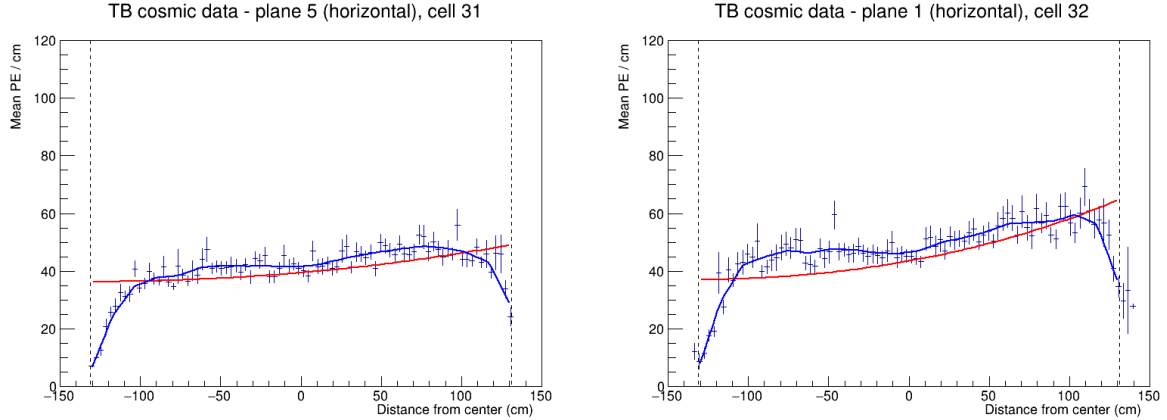


Figure 28: Fit to the energy response in epochs 3 a, b and c. Some underfilled cells that have been refilled in epochs 3b and 3c are now calibrated as shown on the left plot. Cell 32 in plane 1 is the only neighbouring cell to the underfilled cell that didn't manage to get calibrated due to low number of events.

358 usual, it's also the top half of plane 36, which has about $2.5 \times$ larger response as its neighbours.
 359 This could mean that the FEB in plane 36 was faulty only for a limited time compared to the
 360 FEB in plane 58. The energy deposition for these cells is shown on figure 29.

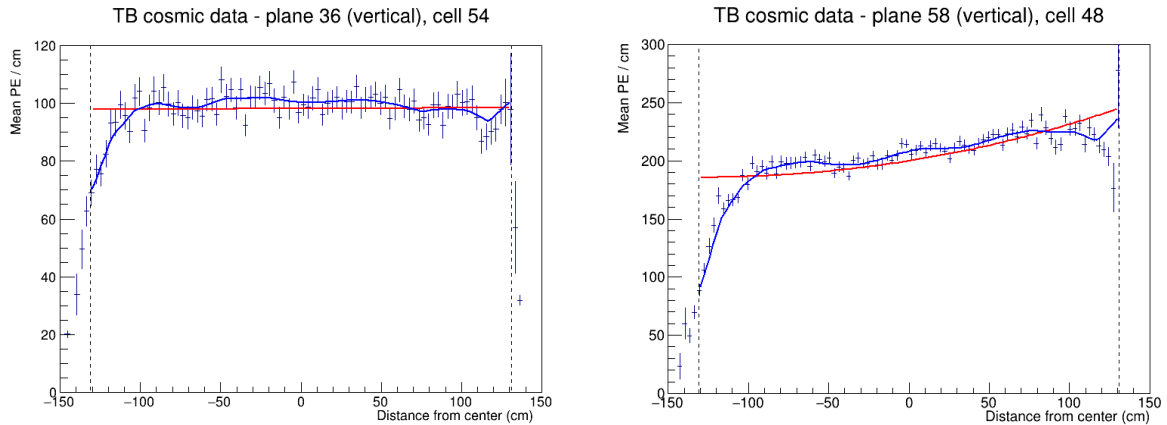


Figure 29: Fit to the energy response in epochs 3 a, b and c. The most obvious faulty FEBs that have a significantly larger energy response than their neighbours.

361 Similarly as in period 2, there are a few cell in the back of the detector that have a sharp
 362 rise in the energy response at the edge of the cell, which causes them to be uncalibrated. This
 363 can be seen on figure 30.

364 **Combined epochs 3d and 3e relative calibration results**

365 The results of the attenuation fits for epochs 3 d and e are shown on figure 31. There we can
 366 see the expected uncalibrated cells in plane 17 related to the dead channel (or possibly still
 367 underfilled cell). The energy deposition for this cell and one of its neighbours is shown on
 368 figure 32.

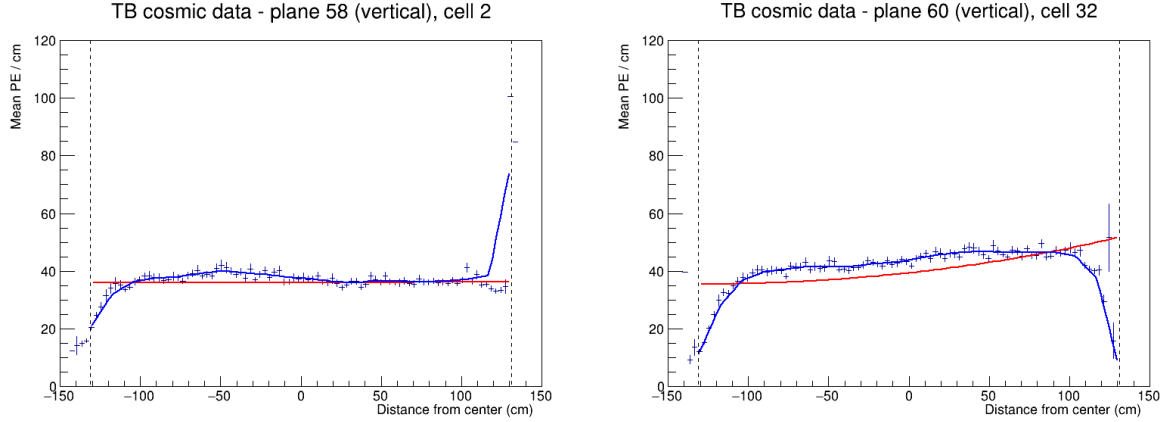


Figure 30: Fit to the energy response in epochs 3 a, b and c. Some cells are not calibrated due to large fluctuations at one edge of the cells.

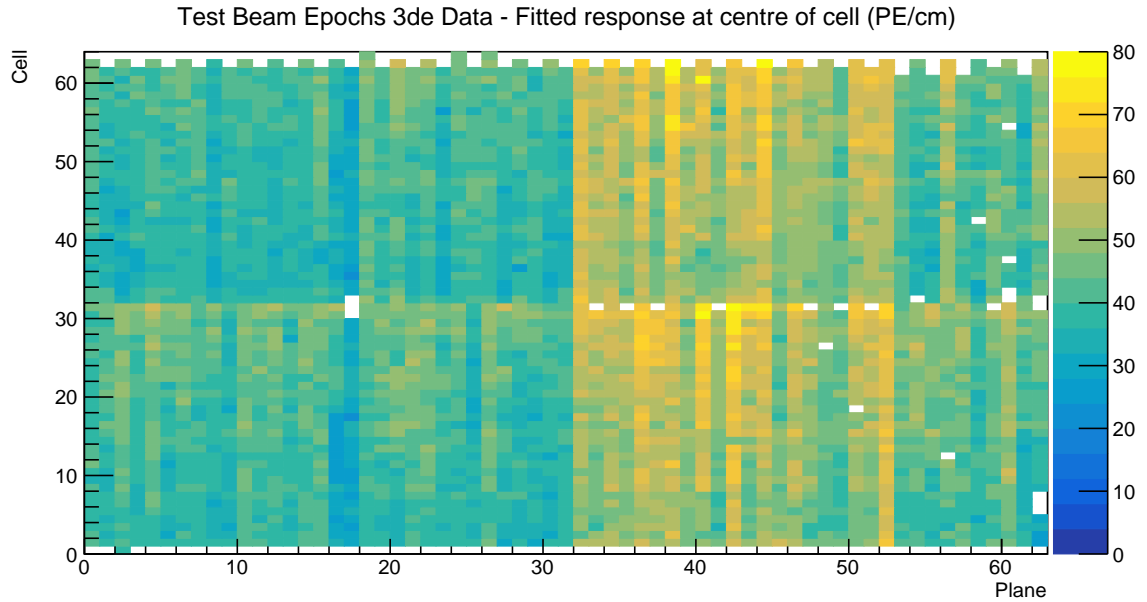


Figure 31: Overview of the relative calibration results for the Teast Beam detector period 3, combined epochs 3d and 3e data. Each cell represents the result fo the attenuation fit to the energy response in the centre of that cell. The blank cells are uncalibrated.

369 Epochs 3 d and e should have all the previously underfilled cells now refilled, but as can be
 370 seen on figure 31, there's several of these cells that are still uncalibrated. The energy deposition
 371 in these cells is shown on figure 33. We can see that these cells have a fairly large discrepancy
 372 between the left and right side of the cells. This is caused by using different scintillator oils for
 373 the initial filling of the cells and for the refilling. Specifically, these cells have been initially
 374 filled with the Ash River and the Texas oils, which have higher energy depositions compared
 375 to the NDOS oil that was used for the refilling. These oils clearly didn't mix properly which
 376 causes a different energy deposition in different parts of the cells. Since this is a physical effect
 377 that should be accounted for in the calibration and as we can see the fits are actually performing
 378 pretty well and are just confused by the unusual shape. We have therefore decided to manually

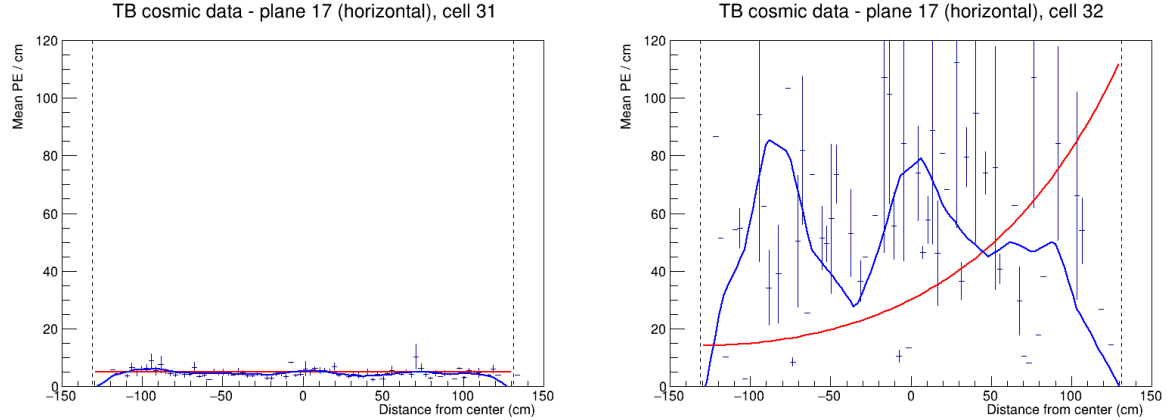


Figure 32: Fit to the energy response in epochs 3 d and e. Possibly dead channel or still underfilled cell.

379 change the χ^2 inside the cvs tables (results of the attenuation fits), so that the $\chi^2 < 0.2$ and
 380 these cells are considered calibrated.

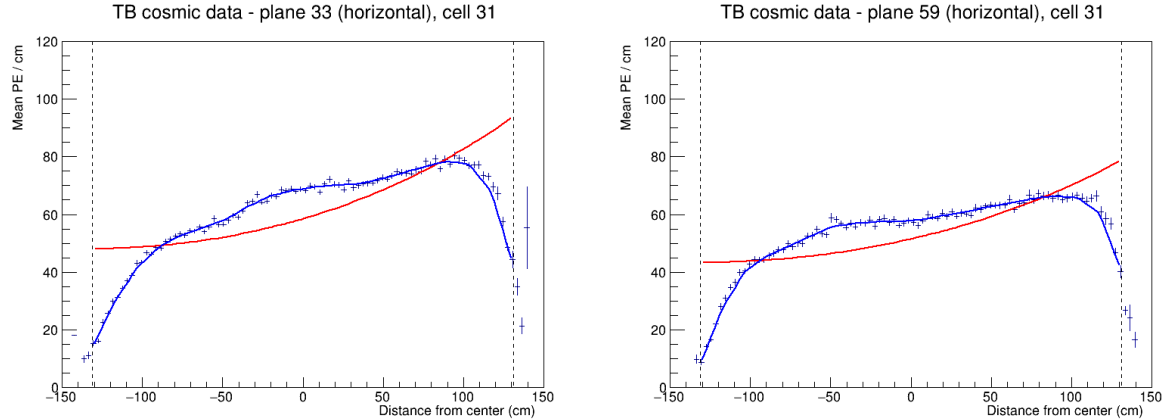


Figure 33: Fit to the energy response in epochs 3 d and e. The scintillator oil used for refilling of the underfilled cells has lower energy response than the oil used for the initial filling. These oils didn't mix properly causing a different energy response in the left and right side of the cell.

381 Some of the cells in the back of the detector have a rise, or drop in energy deposition at the
 382 edge of the cell, as can be seen on figure 34. This is similar to the effect seen in period 2 and
 383 epochs 3abc and since it's again concentrated in the end of the detector we ignored these cells
 384 and left them uncalibrated.

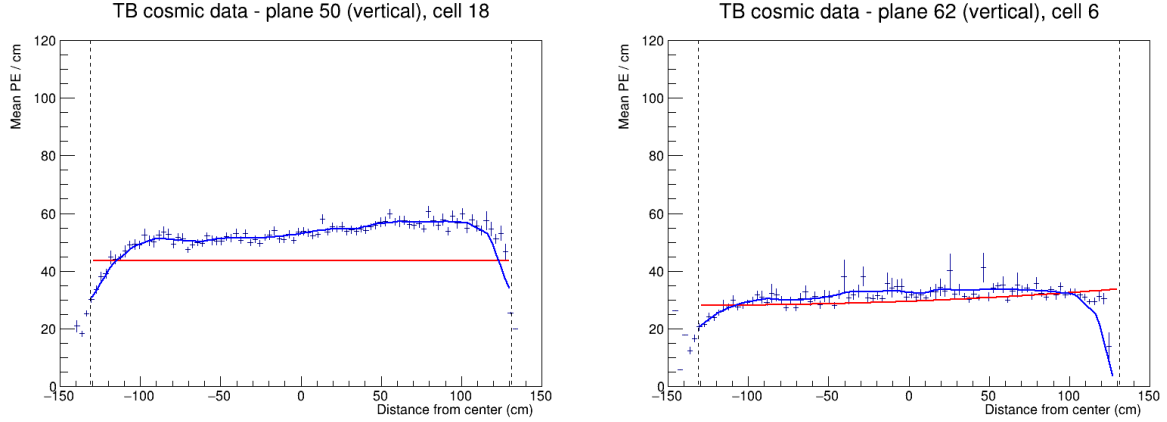


Figure 34: Fit to the energy response in epochs 3 d and e. Some cells have a drop, or a rise of energy response at the edge of the cell. This can be cause by low statistics.

385 4.7 Period 4

386 The period 4 Test Beam data taking period is the best data we managed to collect with almost an
 387 ideal condition of the detector. There's only a few commissioning runs in the very beginning,
 388 which uncovered some dead channels or faulty FEBs that have been fixed. These runs make
 389 epoch 4a shown on the top plot of figure 35.

390 There has also been a cell masking study [reference], during which we masked parts of the
 391 front of the detector to help with FEB saturation. We can clearly see this on the middle plot of
 392 figure 35.

393 Figures 36, 37 and 38 show that the epoch 4a and the cell masking study did have a notice-
 394 able impact on the energy deposition across the detector. We have therefore decided to ignore
 395 these runs and only use the rest of the period 4 data for the calibration.

396 Period 4 relative calibration results

397 Results of the attenuation fits for period 4 are summarised on figure 39.

398 We can see that majority of the detector is calibrated, besides some cells on the edge of the
 399 detector, a few formerly underfilled cells (left plot on figure 40) and one cell with an unusually
 400 high response at the edge of the cell (right plot on figure 40). We treated the formerly underfilled
 401 cells the same way as in epochs 3 d and e, by manually changing their χ^2 to be < 0.2 and
 402 therefore making them calibrated.

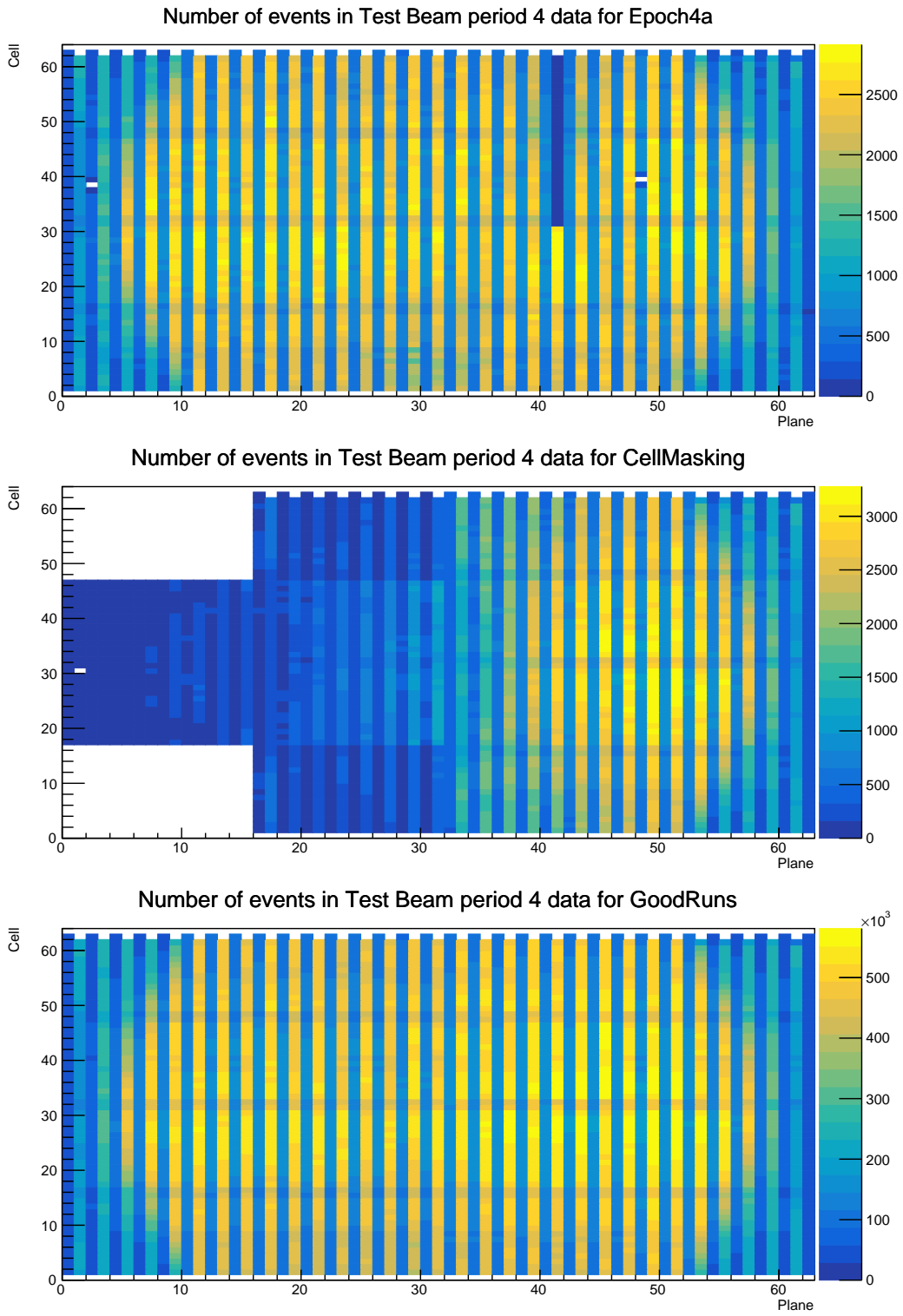


Figure 35: Distribution of events in the Test Beam period 4 data calibration sample. The top plot shows the first three commissioning runs, the middle plot the status of the detector during the Cell Masking studies and the bottom plot shows the rest.

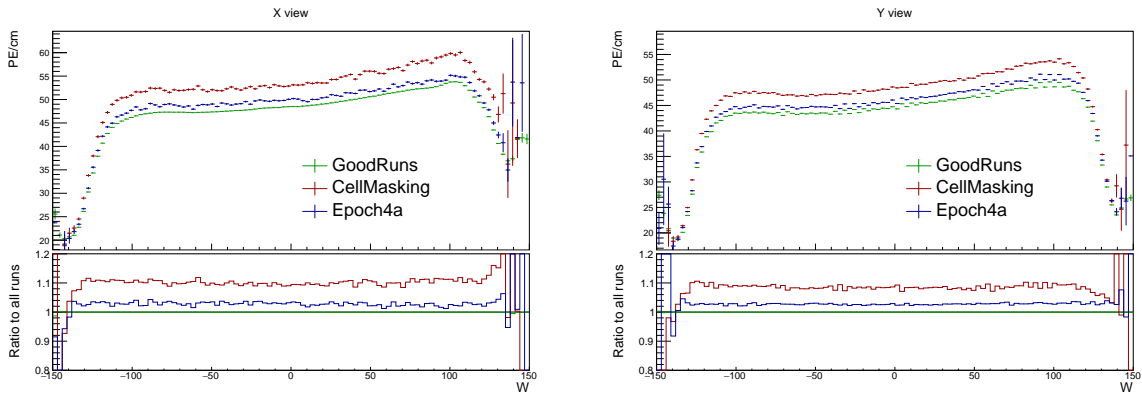


Figure 36: Uncorrected average energy response as a function of the position within a cell (w) for epochs in period 4.

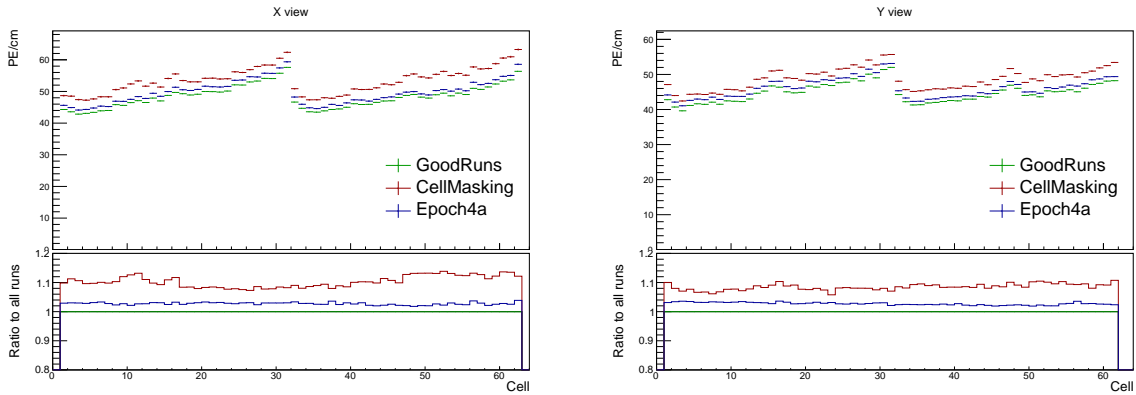


Figure 37: Uncorrected average energy response as a function of cells for epochs in period 4.

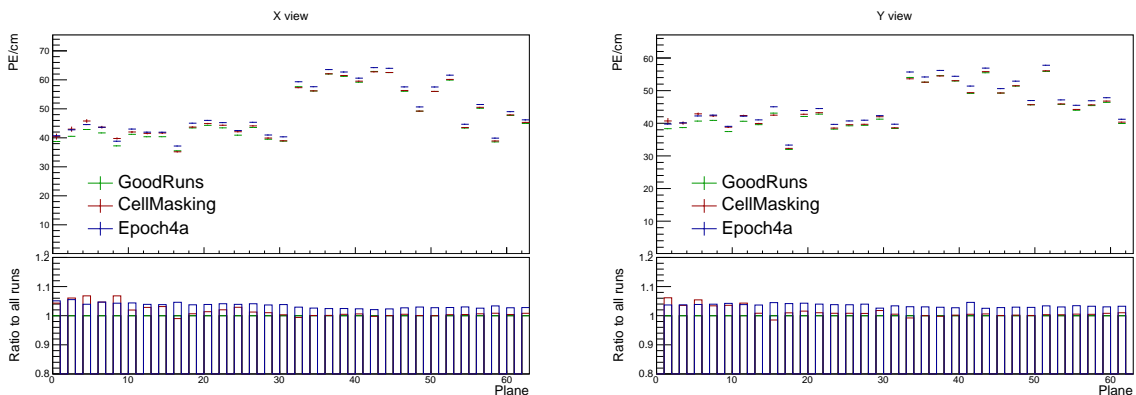


Figure 38: Uncorrected average energy response as a function of planes for epochs in period 4.

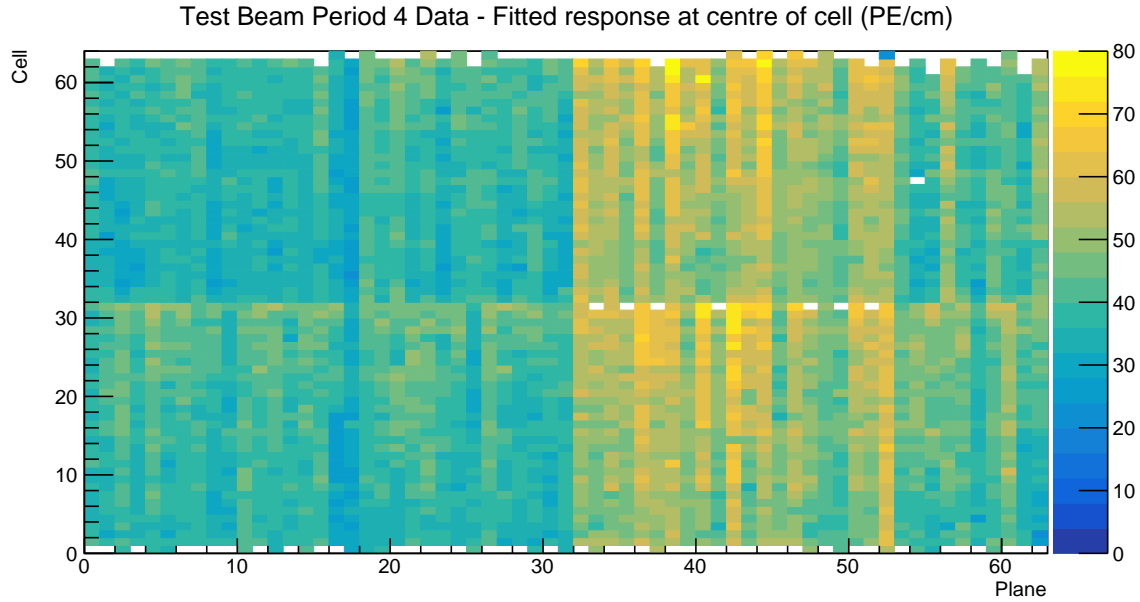


Figure 39: Overview of the relative calibration results for the Teast Beam detector period 4 data. Each cell represents the result fo the attenuation fit to the energy response in the centre of that cell. The blank cells are uncalibrated.

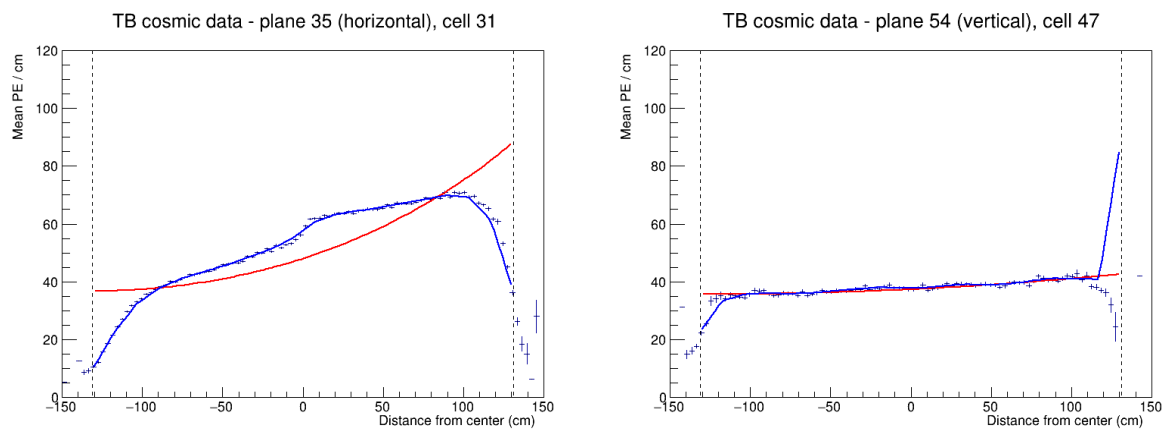


Figure 40: Fit to the energy response in period 4. Previously underfilled cells refilled with a scintillator of a different quality causing an unusual distribution of energy deposition (left). Unusually high energy response at the edge of the cell 47 (right).

⁴⁰³ **4.8 Absolute calibration results**

⁴⁰⁴ TO DO: add description of the absolute calibration results, correct the table to fit the page

| Sample | NHitsx | MEUx | NHitsy | MEUy | MEU | MEU Err | TrueE/dx | tE/dx Err |
|-----------------|-----------|-------|-----------|-------|-------|----------|----------|-----------|
| epoch 3abc data | 2.638e+05 | 38.49 | 1.621e+06 | 39.4 | 38.94 | 0.006758 | 1.772 | 0.000238 |
| epoch 3de data | 1.049e+05 | 38.63 | 6.725e+05 | 39.42 | 39.02 | 0.01048 | 1.772 | 0.000238 |
| period 2 data | 2.322e+05 | 38.7 | 1.413e+06 | 39.4 | 39.05 | 0.007252 | 1.772 | 0.000238 |
| period 4 data | 5.268e+05 | 38.63 | 3.316e+06 | 39.4 | 39.01 | 0.004703 | 1.772 | 0.000238 |
| simulation | 2.829e+05 | 40.17 | 1.842e+06 | 39.93 | 40.05 | 0.006418 | 1.772 | 0.000238 |

⁴⁰⁵

⁴⁰⁶ **4.9 Results**

⁴⁰⁷ TO DO: talk about where are the results and what is the final calibration tag

⁴⁰⁸ **4.10 Validation**

⁴⁰⁹ TO DO: describe the validation plots and possibly add more plots

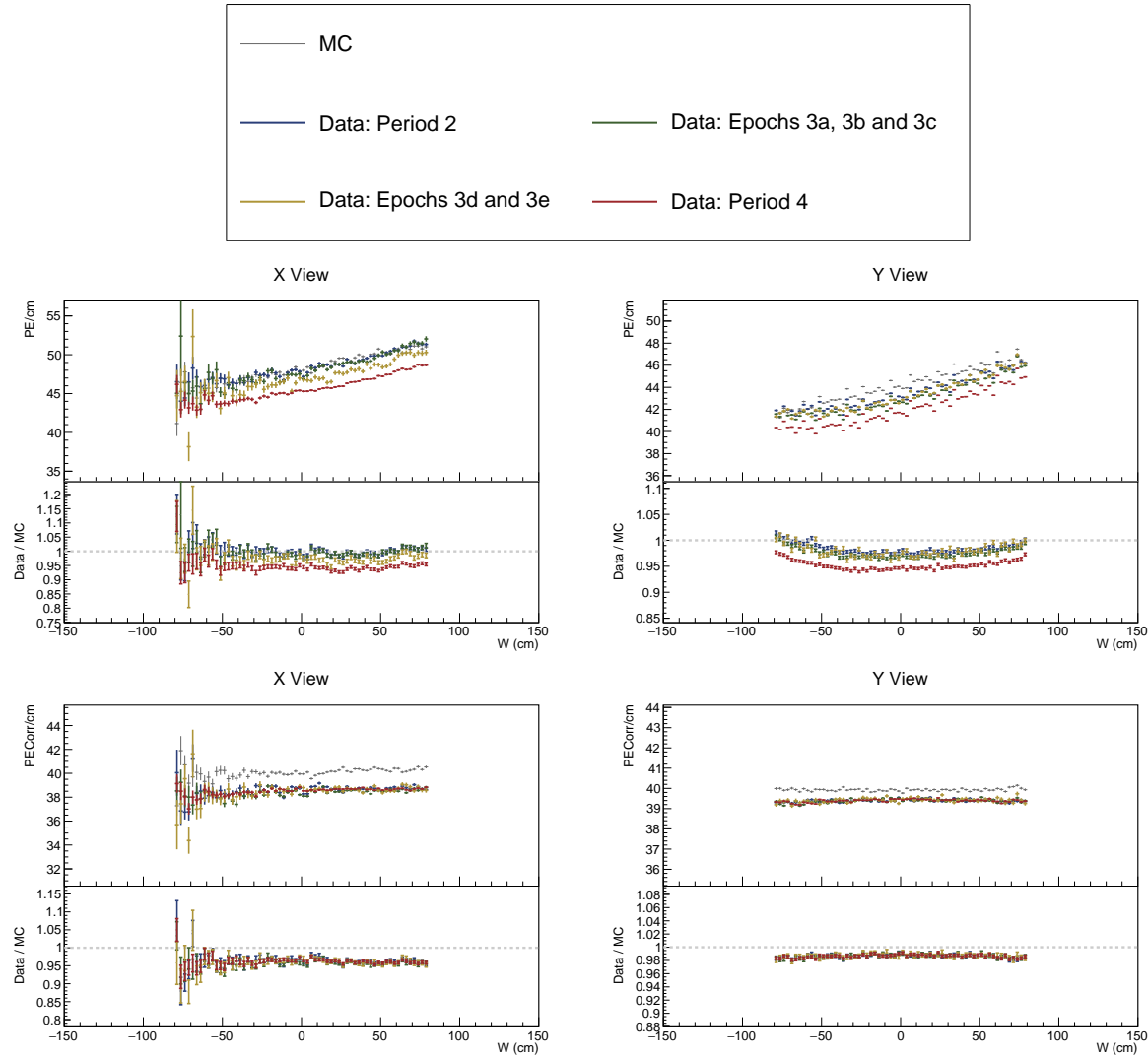


Figure 41: ...

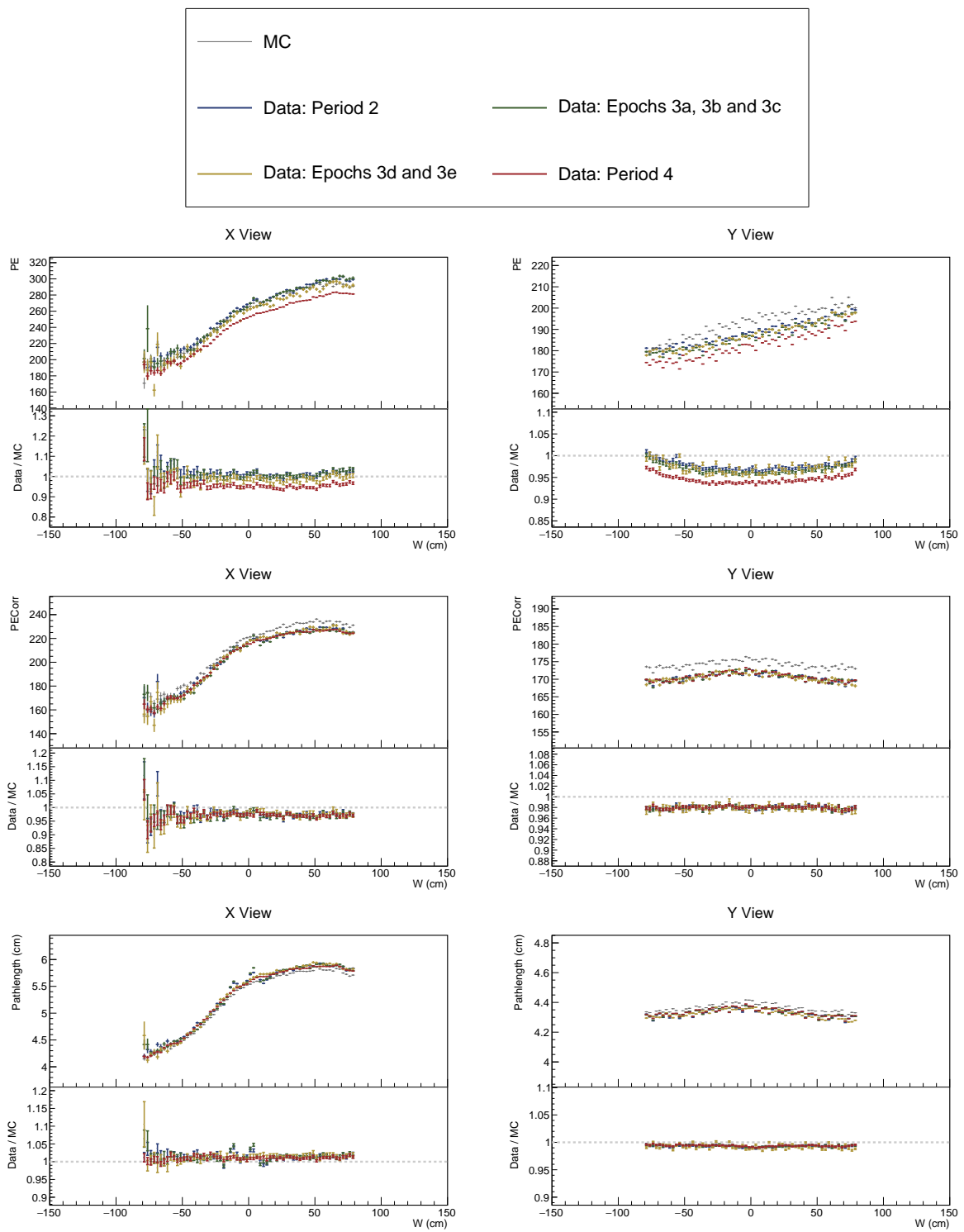


Figure 42: ...

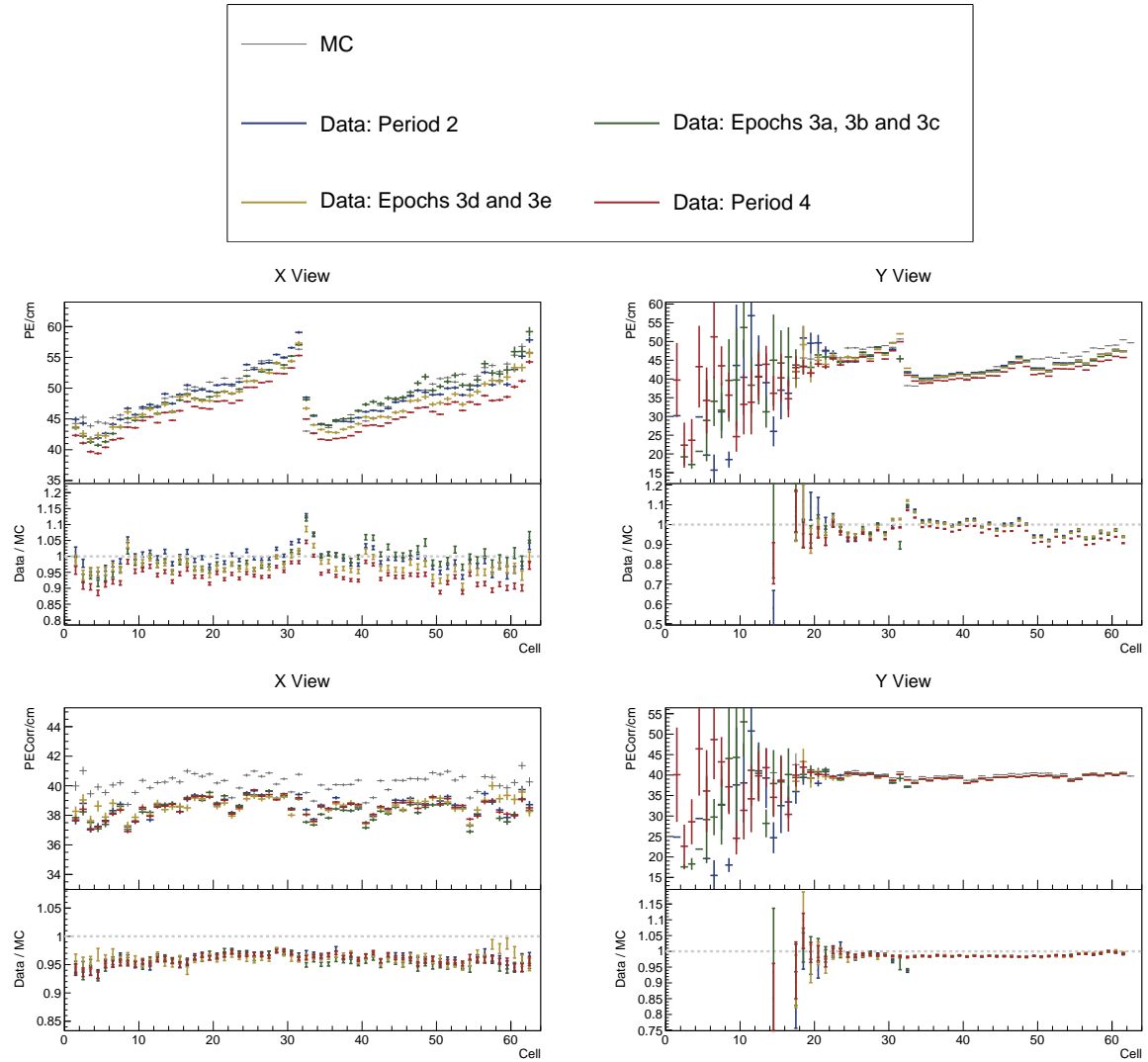


Figure 43: ...

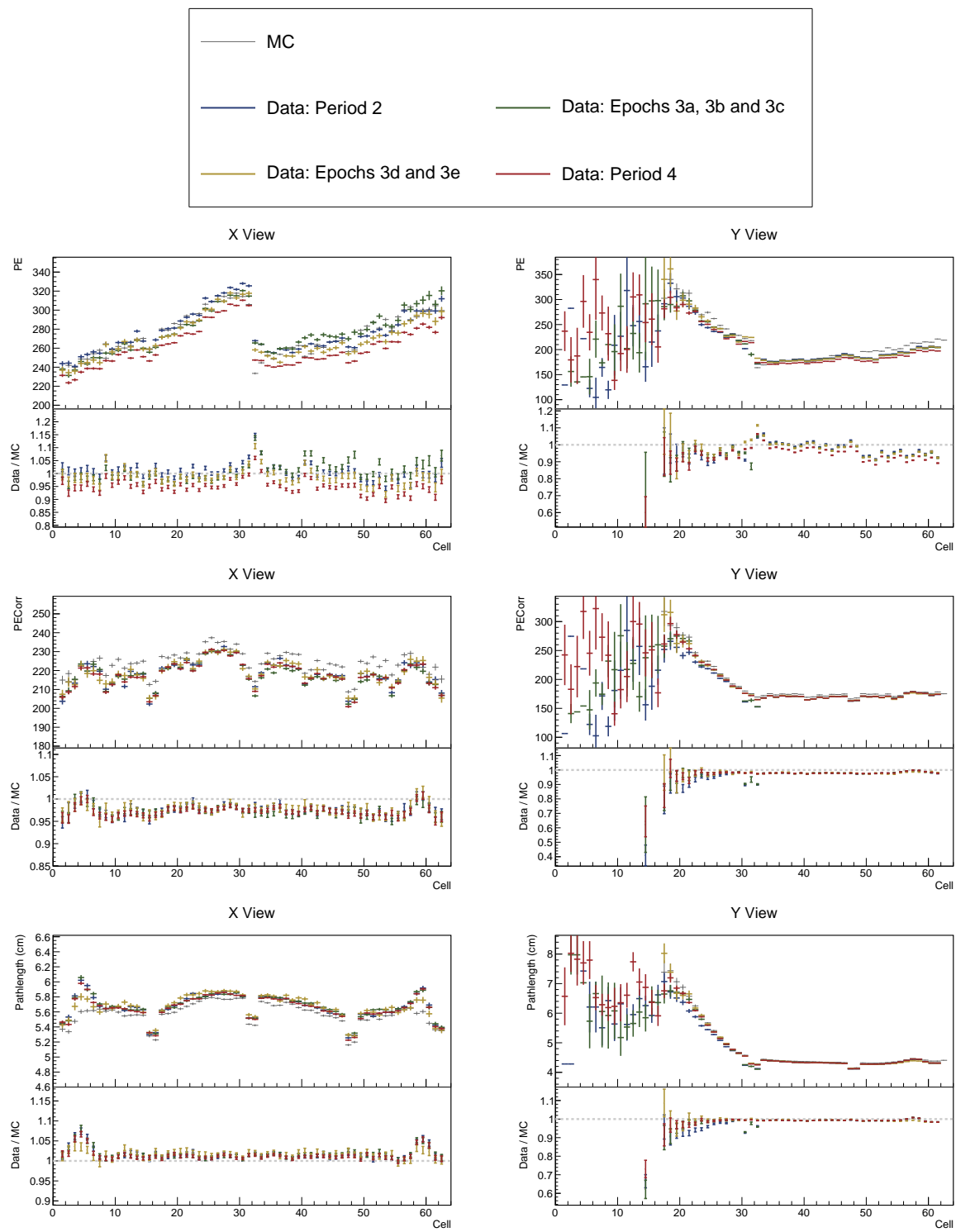


Figure 44: ...

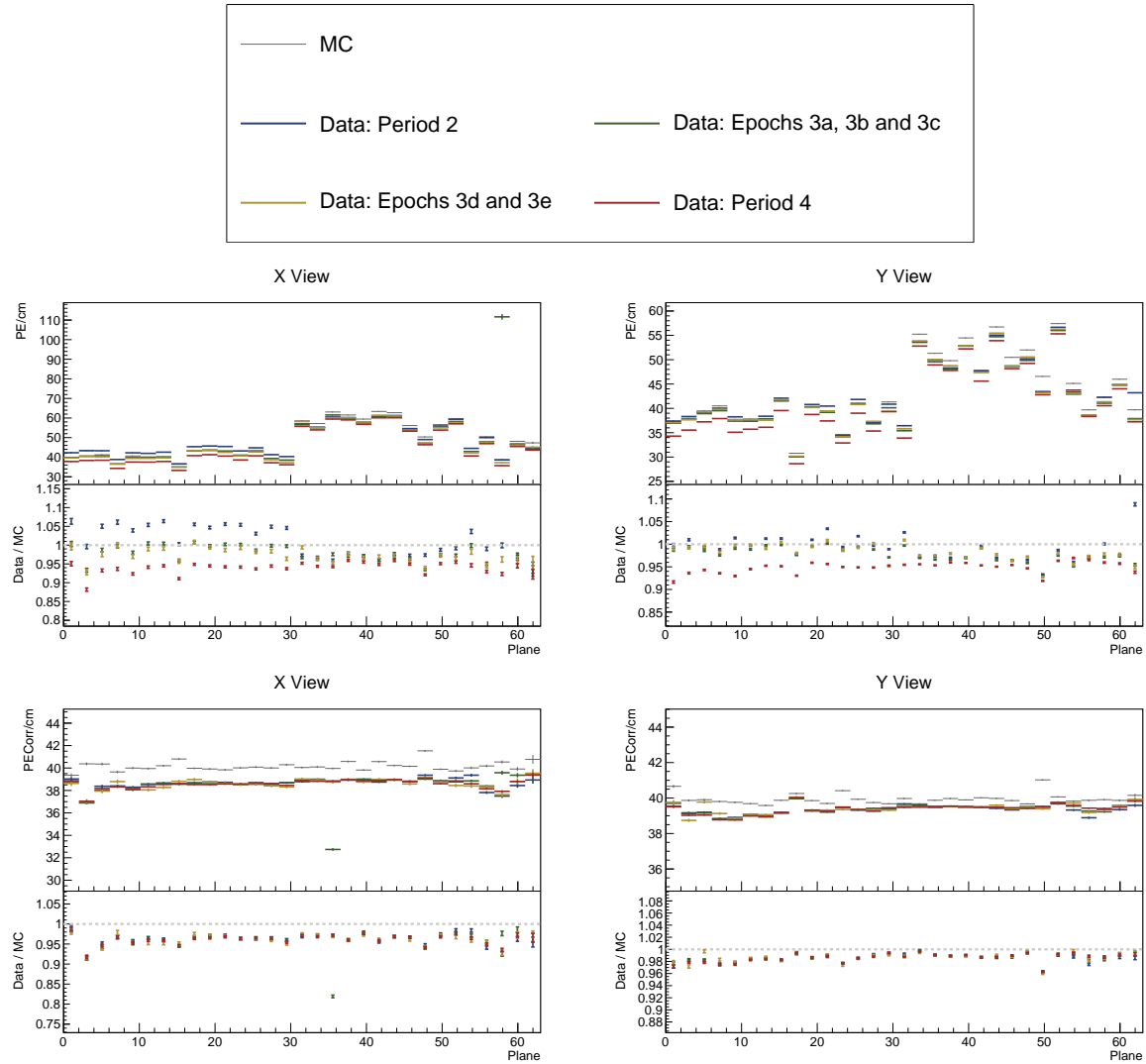


Figure 45: ...

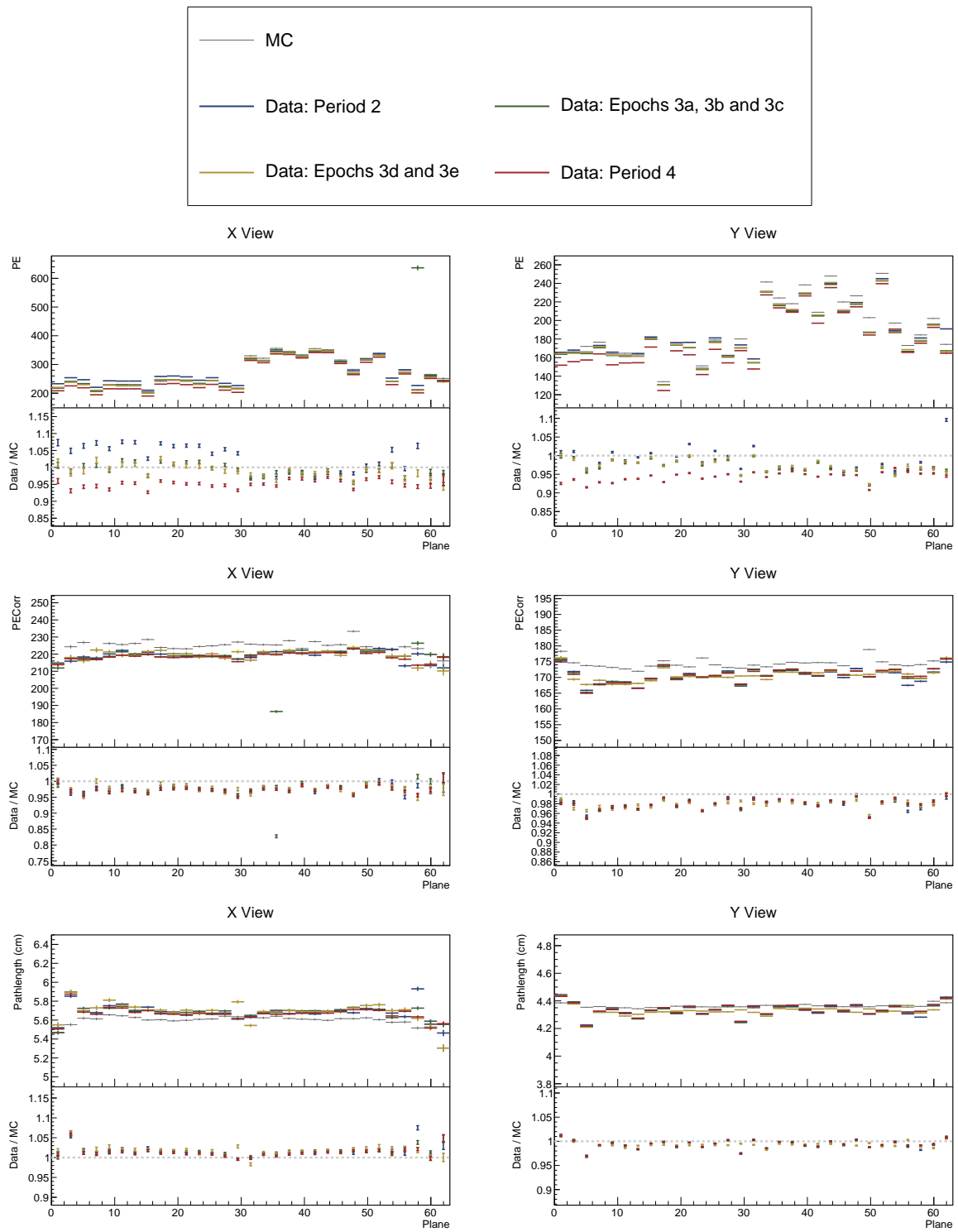


Figure 46: ...

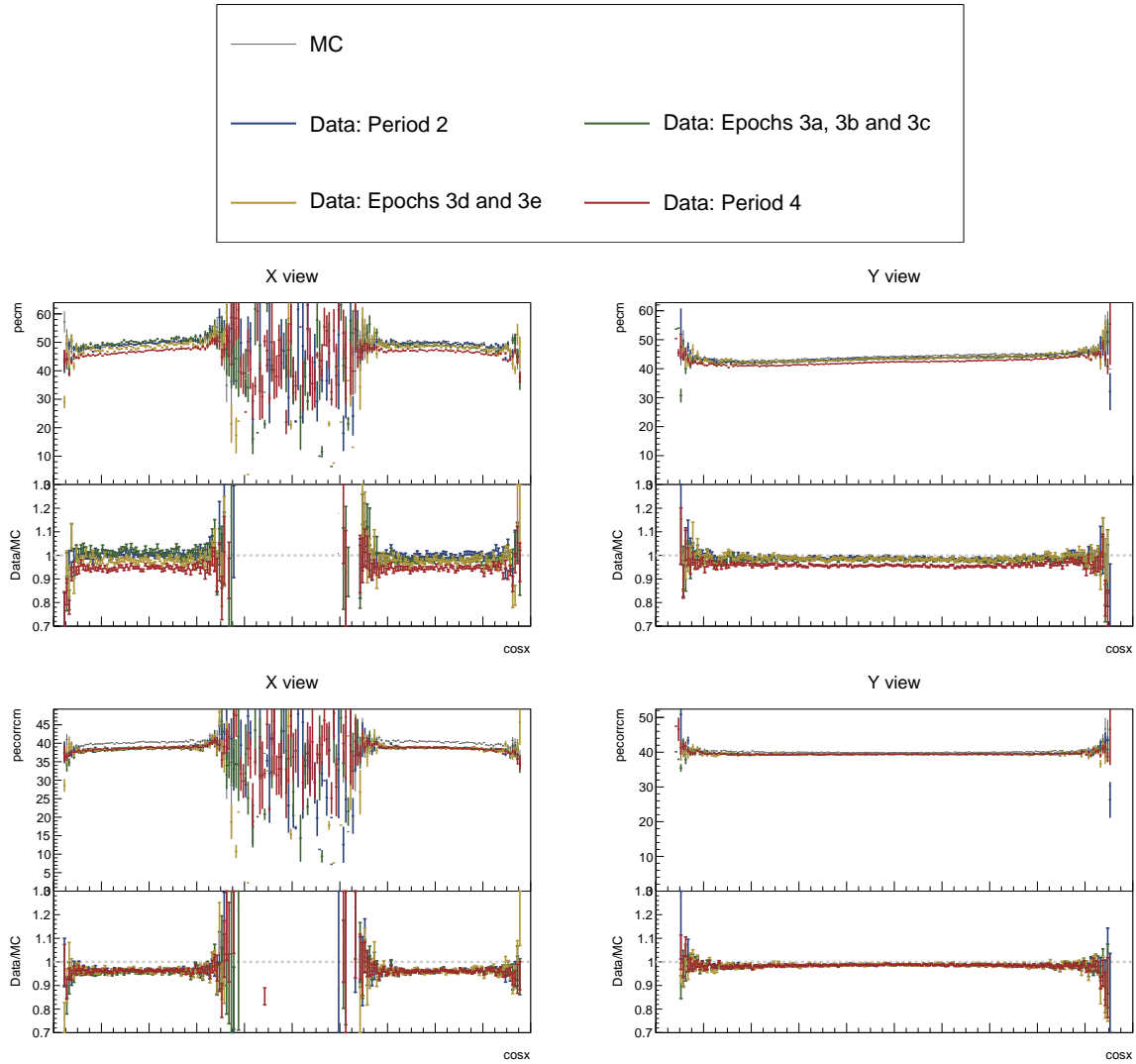


Figure 47: ...

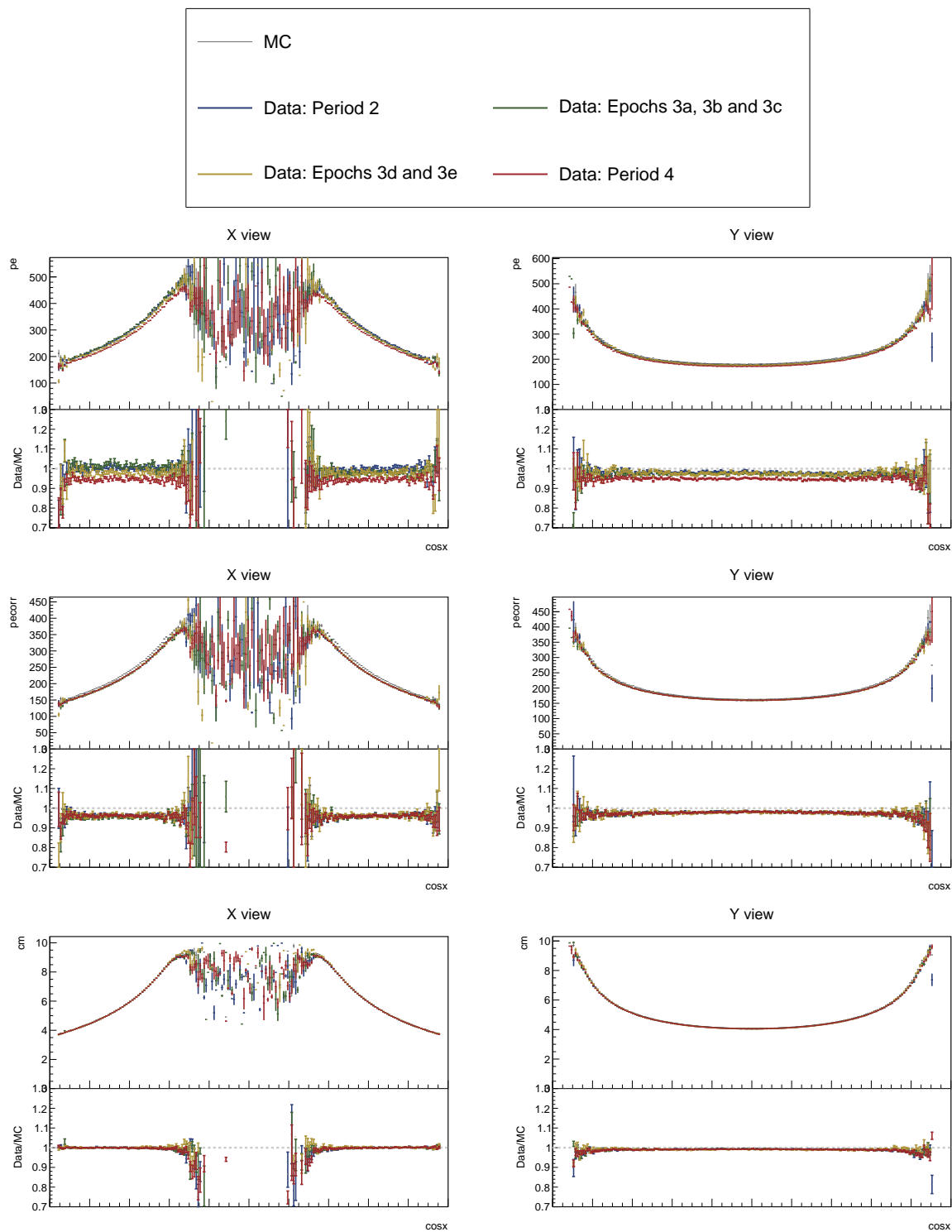


Figure 48: ...

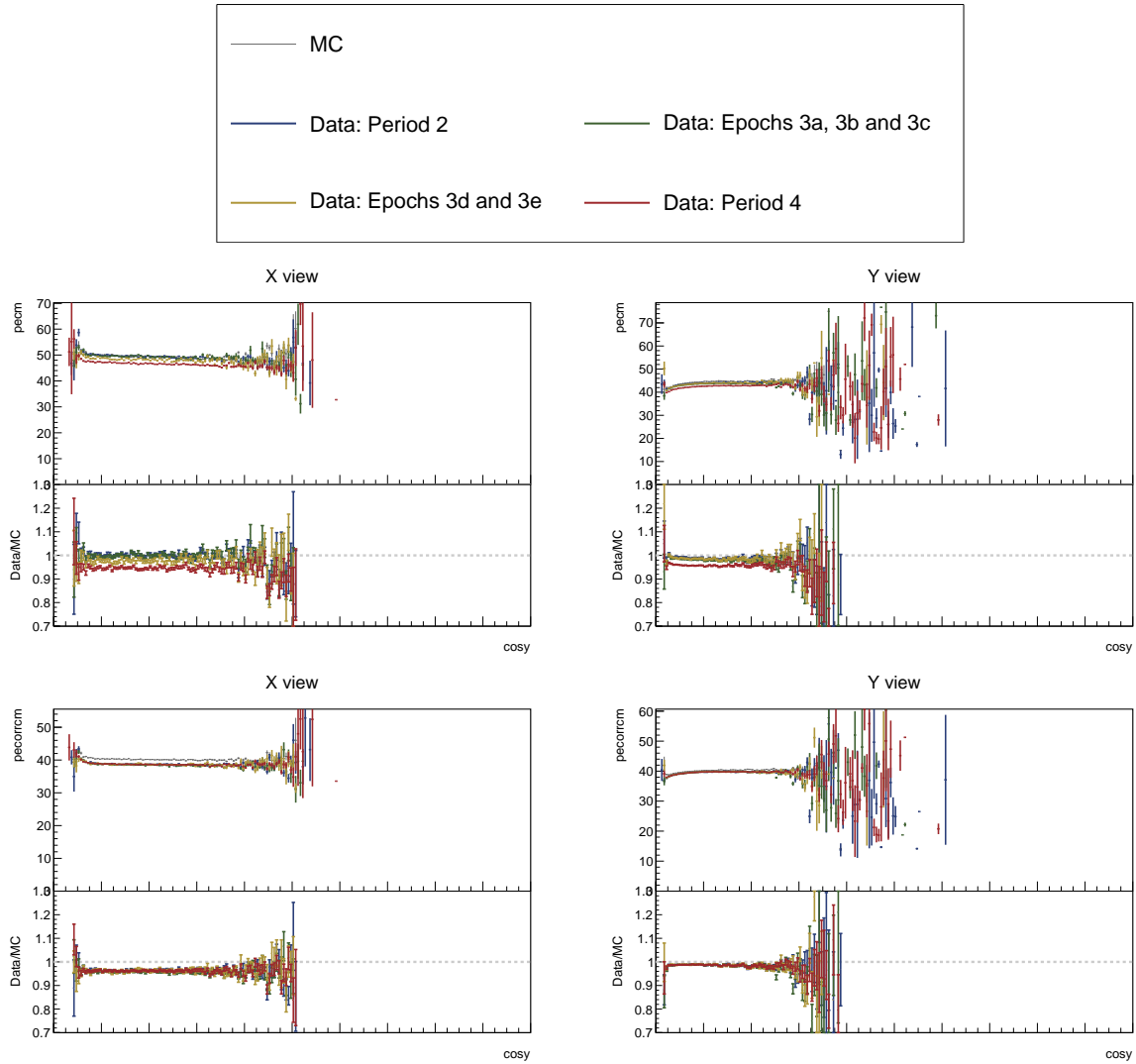


Figure 49: ...

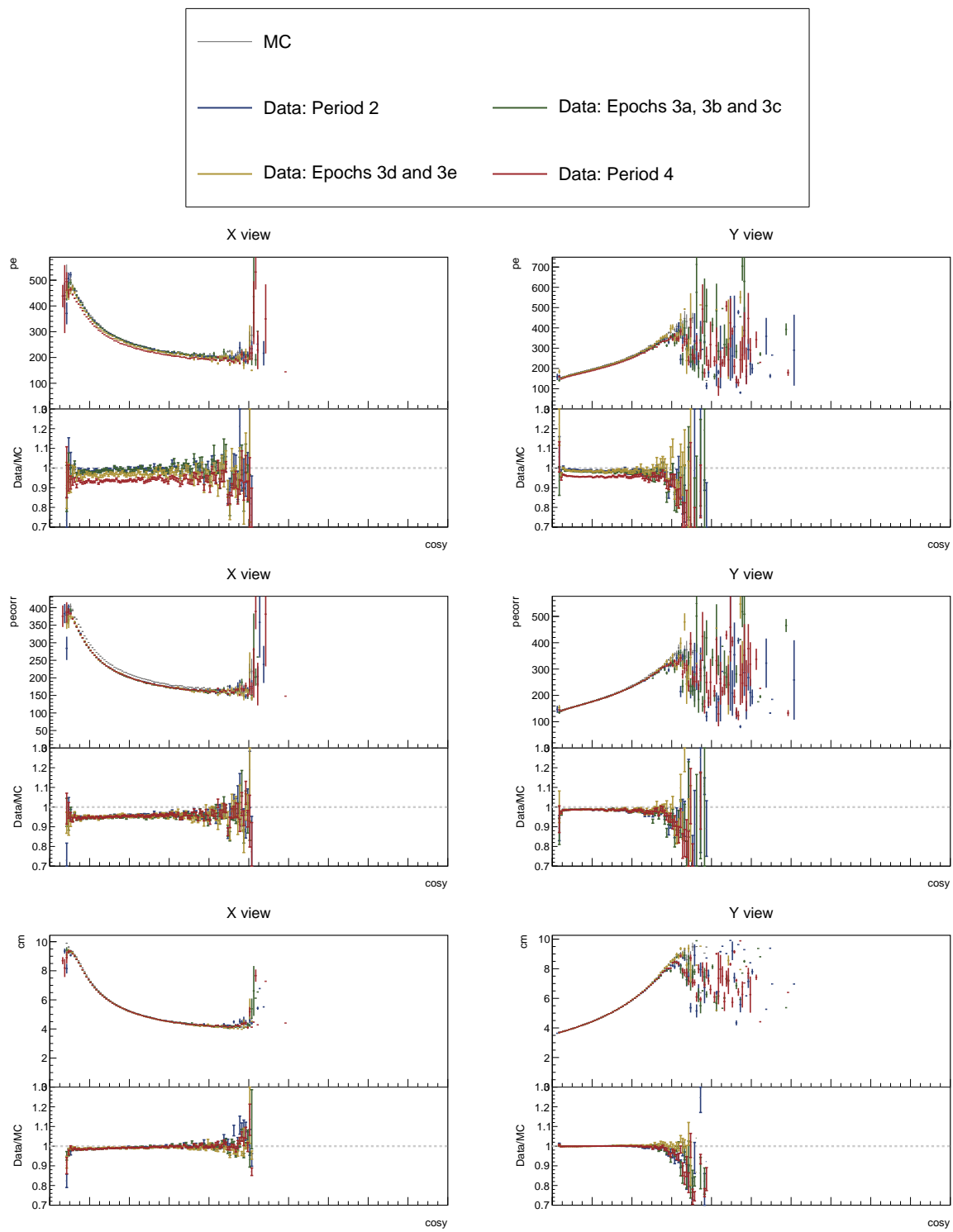


Figure 50: ...

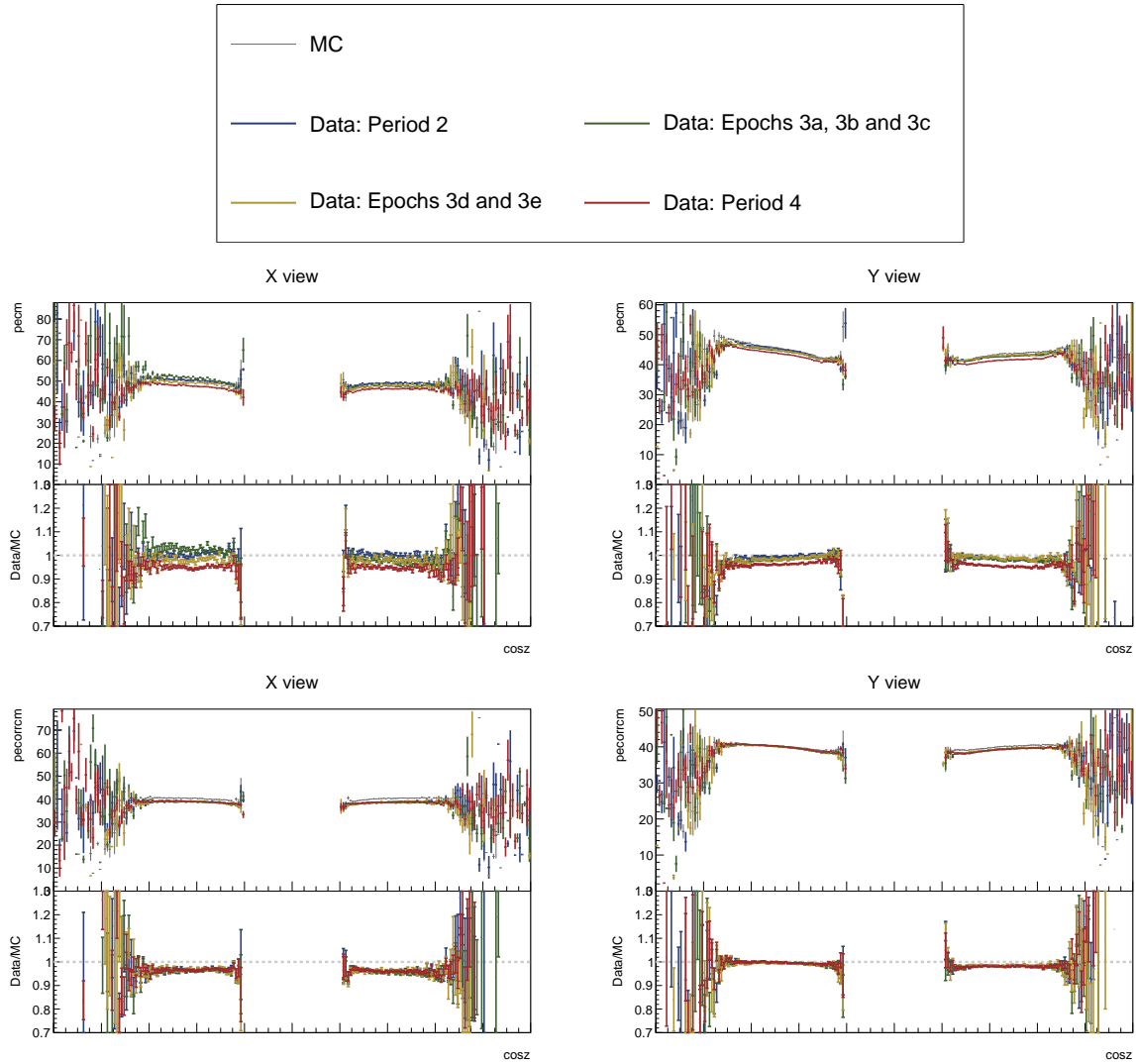


Figure 51: ...

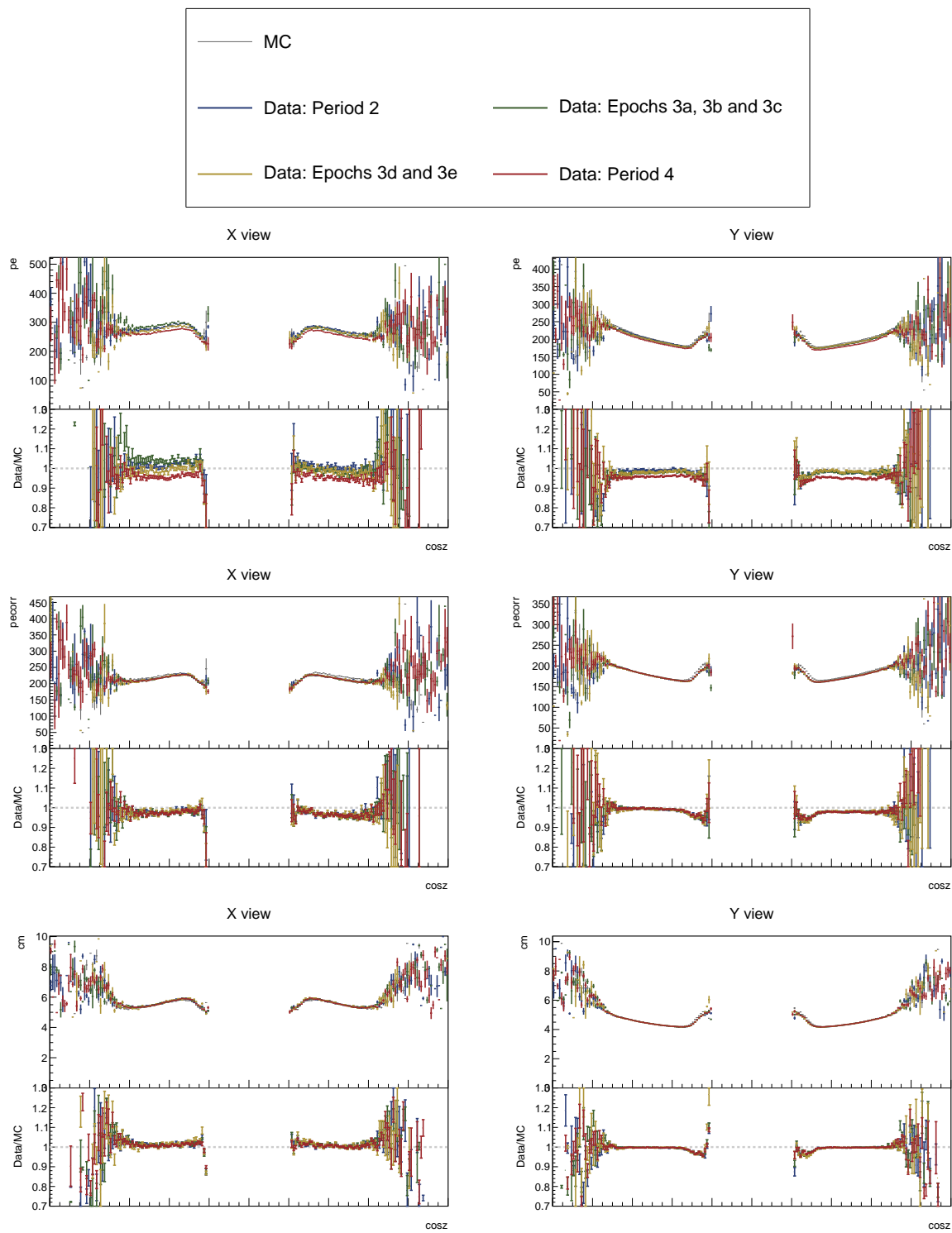


Figure 52: ...

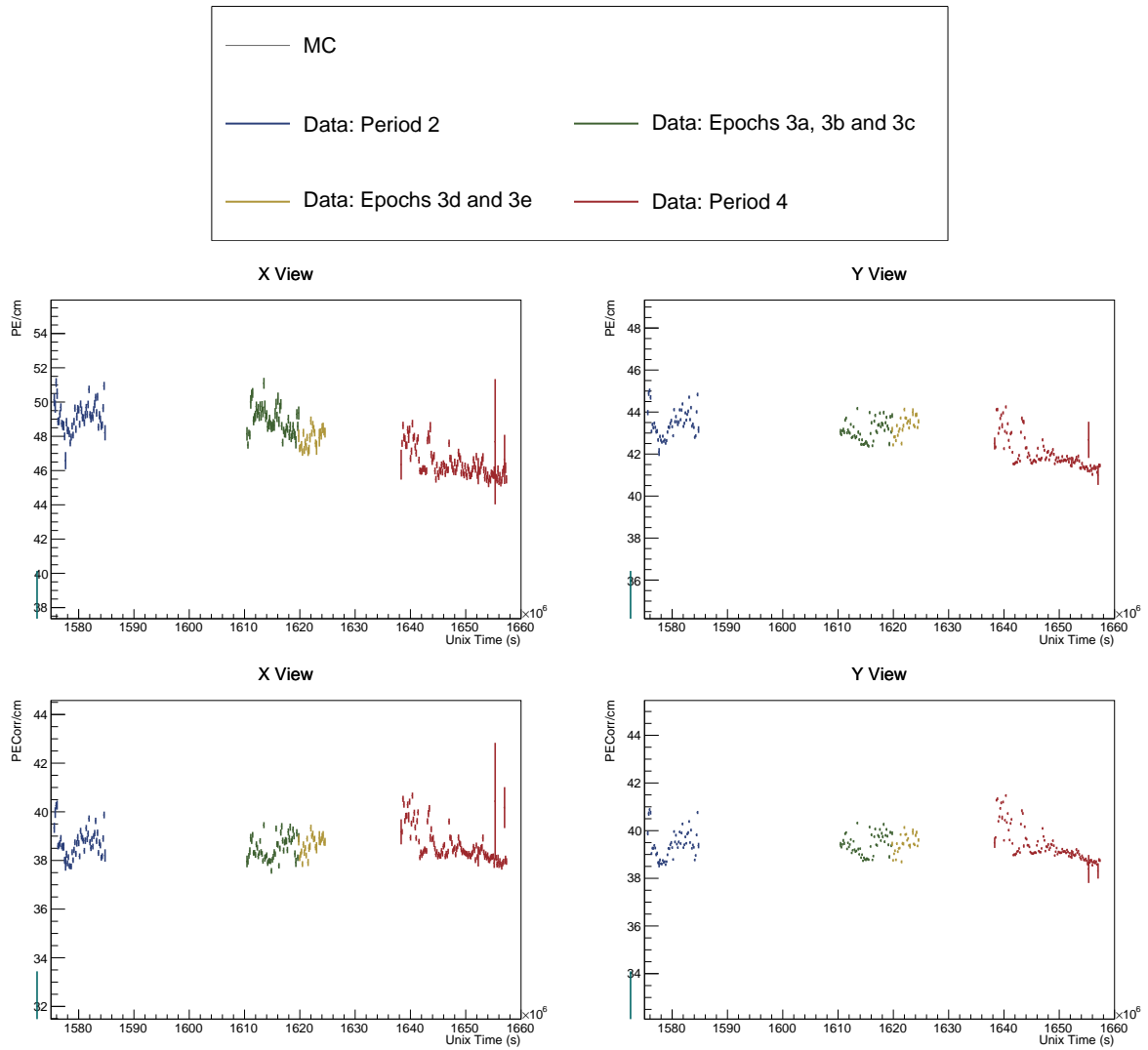


Figure 53: ...

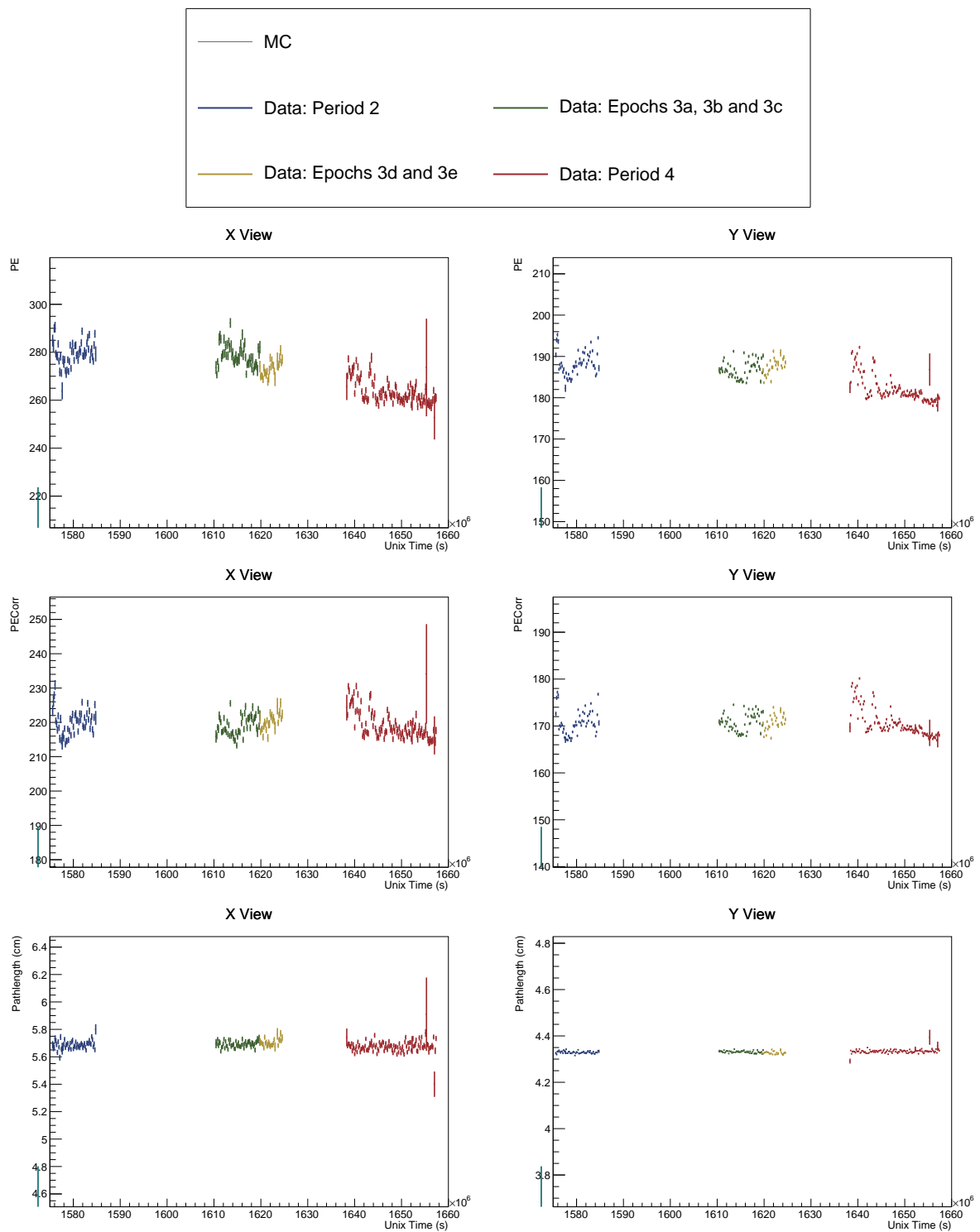


Figure 54: ...

410 **5 Conclusion**

411 TO DO: Write a conclusion

412 **References**

- 413 [1] Alex Sousa. NOvA Test Beam Status and Plans - Support Documentation. NOVA Doc-
414 ument 22172-v2, October 2017. NOvA technical note. URL: <https://nova-docdb.fnal.gov/cgi-bin/sso>ShowDocument?docid=22172>.
- 416 [2] Alex Sousa. NOvA Test Beam Plenary @ IU Collaboration Meeting. NOVA Document
417 29543, May 2018. NOvA internal document. URL: <https://nova-docdb.fnal.gov/cgi-bin/sso>ShowDocument?docid=29543>.
- 419 [3] Michael Wallbank. Final Test Beam Updates (Geometry and Other!). NOVA Document
420 58388, April 2023. NOvA internal document. URL: <https://nova-docdb.fnal.gov/cgi-bin/sso>ShowDocument?docid=58388>.
- 422 [4] Michael Wallbank. Understanding, Improving, Validating the Test Beam Geometry.
423 NOVA Document 57955, February 2023. NOvA internal document. URL: <https://nova-docdb.fnal.gov/cgi-bin/sso>ShowDocument?docid=57955>.
- 425 [5] Robert Kralik. Test beam calibration update. NOVA Document 57516-v2, January
426 2023. NOvA internal document. URL: <https://nova-docdb.fnal.gov/cgi-bin/sso>ShowDocument?docid=57516>.
- 428 [6] Alex Sousa. Test Beam Scintillator Fill Plan. NOVA Document 34196, November
429 2018. NOvA internal document. URL: <https://nova-docdb.fnal.gov/cgi-bin/sso>ShowDocument?docid=34196>.
- 431 [7] Alex Sousa. Test Beam Plenary Update - Jun. 6, 2019. NOVA Document 38349, June
432 2019. NOvA internal document. URL: <https://nova-docdb.fnal.gov/cgi-bin/sso>ShowDocument?docid=38349>.
- 434 [8] Alex Sousa. Test Beam Plenary Update - FNAL September 2018. NOVA Document
435 33012, September 2018. NOvA internal document. URL: <https://nova-docdb.fnal.gov/cgi-bin/sso>ShowDocument?docid=33012>.
- 437 [9] Alex Sousa. 2nd Block Filling Status - Nov. 18, 2019. NOVA Document 41961, Novem-
438 ber 2019. NOvA internal document. URL: <https://nova-docdb.fnal.gov/cgi-bin/sso>ShowDocument?docid=41961>.
- 440 [10] Alex Sousa. Filling System and Scintillator Status. NOVA Document 34067, November
441 2018. NOvA internal document. URL: <https://nova-docdb.fnal.gov/cgi-bin/sso>ShowDocument?docid=34067>.
- 443 [11] Junting Huang, Will Flanagan, and Beatriz Tapia Oregui. Test Beam: Light Yield of
444 the Liquid Scintillator Drained from the NDOS Detector. NOVA Document 38740, July
445 2019. NOvA internal document. URL: <https://nova-docdb.fnal.gov/cgi-bin/sso>ShowDocument?docid=38740>.

- 447 [12] Dung Phan. Test Beam: Tintometer Measurement of Texas A&M oil. NOVA Document
448 39088, July 2019. NOvA internal document. URL: <https://nova-docdb.fnal.gov/cgi-bin/sso>ShowDocument?docid=39088>.
- 450 [13] Teresa Megan Lackey. *Proton Scattering in NOvA Test Beam*. PhD thesis, Indiana U.,
451 July 2022.
- 452 [14] David Northacker, Alex Sousa, and Yagmur Torun. Test Beam - Overfilling Horizontal
453 Planes. NOVA Document 49439, March 2021. NOvA internal document. URL: <https://nova-docdb.fnal.gov/cgi-bin/sso>ShowDocument?docid=49439>.
- 455 [15] Keith Matera et al. Calibration Technotes. NOVA Document 13579, January
456 2017. NOvA technical note. URL: <https://nova-docdb.fnal.gov/cgi-bin/sso>ShowDocument?docid=13579>.
- 458 [16] Christopher J. Backhouse. Cell-by-cell attenuation calibration of the NOvA detec-
459 tors. NOVA Document 7410, December 2014. NOvA technical note. URL: <https://nova-docdb.fnal.gov/cgi-bin/sso>ShowDocument?docid=7410>.
- 461 [17] Evan David Niner. *Observation of Electron Neutrino Appearance in the NuMI Beam with*
462 *the NOvA Experiment*. PhD thesis, Indiana U., 2015. doi:10.2172/1221353.
- 463 [18] Christopher J. Backhouse. Timing bias introduced by incorrect interpretation of the
464 nanoslice. NOVA Document 13518, June 2015. NOvA technical note. URL: <https://nova-docdb.fnal.gov/cgi-bin/sso>ShowDocument?docid=13518>.
- 466 [19] Luke Vinton. Calorimetric Energy Scale Calibration of the NOvA Detectors. NOVA Doc-
467 ument 13579, document FA_Calorimetric_energy_scale.pdf, July 2015. NOvA technical
468 note. URL: <https://nova-docdb.fnal.gov/cgi-bin/sso>ShowDocument?docid=13579>.
- 470 [20] Keith Matera. Keith's Swell Guide: The Calibration Meta. NOVA Document 13579, doc-
471 ument Calibration_Meta_READFIRST.pdf, January 2017. NOvA technical note. URL:
472 <https://nova-docdb.fnal.gov/cgi-bin/sso>ShowDocument?docid=13579>.
- 473 [21] Christopher Backhouse, Alexander Radovic, and Prabhjot Singh. The Attenuation and
474 Threshold Calibration of the NOvA detectors. NOVA Document 13579, document
475 SA_Attenuation_and_Threshold.pdf, May 2016. NOvA technical note. URL: <https://nova-docdb.fnal.gov/cgi-bin/sso>ShowDocument?docid=13579>.
- 477 [22] Ryan J. Nichol. Fibre brightness from cosmic muon data. NOVA Document 34909, De-
478 cember 2018. NOvA technical note. URL: <https://nova-docdb.fnal.gov/cgi-bin/sso>ShowDocument?docid=34909>.
- 480 [23] Anna Maureen Hall. TB P2 Calib. Summary. NOVA Document 49674, March 2021.
481 NOvA internal document. URL: <https://nova-docdb.fnal.gov/cgi-bin/sso>ShowDocument?docid=49674>.
- 483 [24] Matthew Strait. Update on light level tuning. NOVA Document 43249, February
484 2020. NOvA internal document. URL: <https://nova-docdb.fnal.gov/cgi-bin/sso>ShowDocument?docid=43249>.